AD_____

Award Number: W81XWH-11-1-0270

TITLE: Enhancement of Radiation Therapy in Prostate Cancer by DNA-PKcs Inhibitor

PRINCIPAL INVESTIGATOR: Debabrata Saha, Ph.D.

CONTRACTING ORGANIZATION: University of Texas Southwestern Medical Center
Dallas, TX 75390-7208

REPORT DATE: July 2013

TYPE OF REPORT: Annual

PREPARED FOR: U.S. Army Medical Research and Materiel Command
Fort Detrick, Maryland 21702-5012

REPORT DOCUMENTATION PAGE

Form Approved
OMB No. 0704-0188

1. REPORT DATE	2. REPORT TYPE	3. DATES COVERED
July 2013	Annual	1 July 2012 – 30 June 2013

4. TITLE AND SUBTITLE

Enhancement of Radiation Therapy in Prostate Cancer by DNA-PKcs Inhibitor

5a. CONTRACT NUMBER

5b. GRANT NUMBER
W81XWH-11-1-0270

5c. PROGRAM ELEMENT NUMBER

6. AUTHOR(S)

Debabrata Saha, Ph.D.

E-Mail: Debabrata.Saha@utsouthwestern.edu

5d. PROJECT NUMBER

5e. TASK NUMBER

5f. WORK UNIT NUMBER

7. PERFORMING ORGANIZATION NAME(S) AND ADDRESS(ES)

University of Texas Southwestern Medical Center
Dallas, TX 75390-7208

8. PERFORMING ORGANIZATION REPORT NUMBER

9. SPONSORING / MONITORING AGENCY NAME(S) AND ADDRESS(ES)
U.S. Army Medical Research and Materiel Command
Fort Detrick, Maryland 21702-5012

10. SPONSOR/MONITOR'S ACRONYM(S)

11. SPONSOR/MONITOR'S REPORT NUMBER(S)

12. DISTRIBUTION / AVAILABILITY STATEMENT
Approved for Public Release; Distribution Unlimited

13. SUPPLEMENTARY NOTES

14. ABSTRACT

Prostate cancer (PCa) is the second leading cause of cancer death (~30,000/year) in men in the USA. Surgery and radiotherapy are the most effective therapies to treat PCa patients. However, both these forms of treatment, show significant tumor recurrence with locally aggressive disease, metastasis and the morbidity in patients. Several biological disorders are thought to underlie the cause of prostate cancer. One such factor is a tumor suppressor gene DAB2IP which encodes a member of the Ras-GAP protein family. Genome wide Single Nucleotide Polymorphism (SNP) association studies in a large number of patients indicated that DAB2IP is linked with the risk of aggressive prostate cancer. DAB2IP deficient PCa cells are resistant to radiation treatment. Therefore, to improve radiation killing of these aggressive PCa cells, this proposal will explore the radiosensitizing property of NU7441, a specific kinase inhibitor of DNA-PKcs.

15. SUBJECT TERMS
Radiation therapy, Prostate cancer, Radio-sensitization, DNA-Double strand break, cell cycle

16. SECURITY CLASSIFICATION OF:			17. LIMITATION OF ABSTRACT	18. NUMBER OF PAGES	19a. NAME OF RESPONSIBLE PERSON
a. REPORT	b. ABSTRACT	c. THIS PAGE			USAMRMC
U	U	U	UU	30	19b. TELEPHONE NUMBER *(include area code)*

Front cover,
Standard Form (SF 298),

Table of contents

Introduction

Prostate cancer (PCa) is the second leading cause of cancer death (~30,000/year) in men in the USA. Surgery and radiotherapy are the most effective therapies to treat PCa patients. However, both these forms of treatment, show significant tumor recurrence with locally aggressive disease, metastasis and the morbidity in patients. Several biological disorders are thought to underlie the cause of prostate cancer. One such factor is a tumor suppressor gene DAB2IP which encodes a member of the Ras-GAP protein family. Genome wide Single Nucleotide Polymorphism (SNP) association studies in a large number of patients indicated that DAB2IP is linked with the risk of aggressive prostate cancer. DAB2IP deficient PCa cells are resistant to radiation treatment. Therefore, to improve radiation killing of these aggressive PCa cells, this proposal will explore the radiosensitizing property of NU7441, a specific kinase inhibitor of DNA-PKcs. Three specific aims were proposed:

Aim 1: To test whether a DNA-PKcs inhibitor can radio-sensitize DAB2IP deficient aggressive PCa cells under normoxic and hypoxic conditions.
Aim 2: To study the role of DNA-PKcs in HIF-1α stabilization under hypoxic conditions in DAB2IP deficient prostate cancer cells.
Aim 3: To investigate the combined effect of a DNA-PK inhibitor and radiation therapy in a rodent orthotopic (OT) PCa model using image guided radiation therapy (IGRT).

We have made significant progress towards specific aim 1 and results were described in details in the following sections.

Body:

Following tasks were proposed for the Year 2.

Task 5 (Specific Aim 2.1): Months 10-14
In this specific aim, experiment will be performed in DNA-PKcs knockout human prostate cancer cells that are deficient in DAB2IP. Dr. Hsieh's lab will be responsible for establishing and validating cell lines that will be used in specific aim 2. Dr. Lin will perform this study under Dr. Chen's supervision. Drs. Saha and Chen will monitor the progress of this work and discuss the results during their biweekly meeting.

Task 6 (Specific Aim 2.1): Months 15-18
Once these cell lines are established, we will investigate the mechanism of DNA-PKcs-dependent HIF-1α stabilization under hypoxia. These experiments will be performed primarily by Dr. Lin in Dr. Chen's lab.

Task 7 (Specific Aim 2.1): Months 19-22
To further investigate the role of DNA-PK in HIF-1α stabilization, DNA-PK deficient and proficient prostate cancer cells will be transiently transfected with hypoxia responsive elements fused with an oxygen-dependent-degradation domain (ODD) tagged with luciferase. Series of reports assays will be performed in hypoxic and normoxic condition. This part of study will be performed mostly in Dr. Chen's lab.

Task 8 (progress report and manuscript preparation) Months 22-24
Dr. Saha will prepare the annual report on the 2nd year progress and prepare manuscript focusing on the role of DNA-PKcs on DAB2IP deficient in prostate cancer cell and their response to radiotherapy. Drs. Saha, Chen and Hsieh will closely work on the preparation of the manuscript.

Task 9 (Specific Aim 3.1): Months 22-30
We will investigate the effect NU7441 in combination with radiation in rat orthotopic model. We like to start all the in vivo experiments at the same time in order to minimize the animal usage. Appropriate animals groups will be formed after implanting the DAB2IP deficient prostate cells as mentioned in experimental methods. Dr. Mathur who is an expert in ultrasound guided tumor cell implantation in the rat prostate will lead this study. He along with Dr. Song will perform the image guided radiation into the prostate. Dr. Song will be responsible for treatment planning, dosimetry, dose distribution and he will work under the supervision of Dr. Solberg. Dr. Mathur will administer the drug (NU7441) prior to radiation. After the treatment, Dr. Mathur will measure tumor volume using the ultrasound system and monitor tumor progression and metastasis by bioluminescence imaging. This task will be monitored very closely by Drs. Saha, Mathur, Song and Solberg. The reason this task takes a long time because we are anticipating a significant tumor growth delay in response to combined modality treatment. Statistical analysis will be performed by the Statistician Dr. Xie at our Simmons Cancer Statistical Core.

Key research accomplishments

Last year we reported that the results under Task 1-3 will be published in a peer reviewed journal. We submitted our manuscript in the journal of Neoplasia. Our manuscript was accepted with minor revisions and now available on line (Yu et al, Neoplasia, 2012:1203-1212). In addition, a part of Task 9 is now published in the journal of International Oncology (Tumati et al, 2013). We will attach the accepted manuscript with this report.

Task 5 and Task 6

In this study we used both human prostate (C4-2) and colon (HCT 116) cancer cell lines to investigate the role of DNA-PKcs in HIF-1α stabilization under hypoxic conditions in DAB2IP deficient prostate cancer cells. First we did few key experiments using HCT116 cell lines

Exp 1: HIF-1α induction upon hypoxia is dependent on DNA-PKcs. (A) the parental human colon cancer HCT116 and DNA-PKcs knockout (PKcs-/-) cells were cultured under continuous normoxia (N, 20% O2) condition or were subjected to hypoxic condition (H, 1.0% O2) for 4 hrs. Whole cell lysates were prepared for western blot analysis for HIF-1α and actin. The result showed that hypoxia dependent HIF-1α stabilization is significantly attenuated in DNA-PKcs deficient cells. **(B)** HCT116 and DNA-PKcs-/- cells were subjected to 4 hrs of hypoxia followed by reoxygenation for indicated times. Whole cell lysates were western blot analyzed. The result confirmed that hypoxia induction of HIF-1α is attenuated in DNA-PKcs-/- cells and that reoxygenation hastens HIF-1α degradation in DNA-PKcs-/- cells.

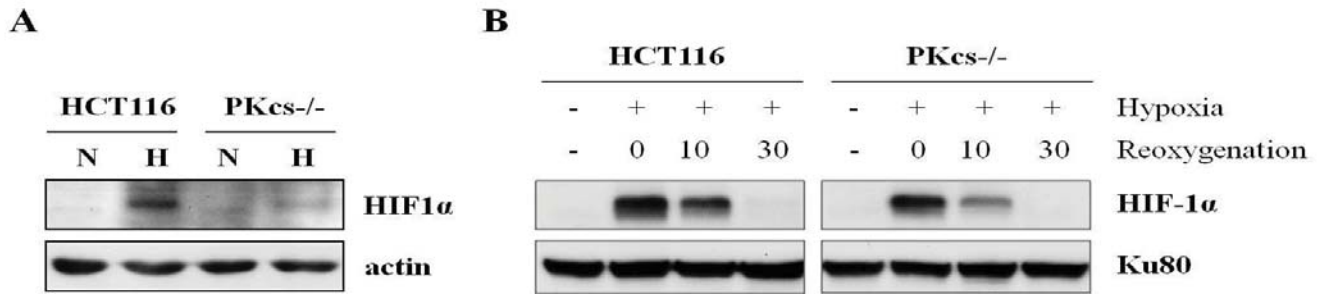

Exp 1: **A**: Westernblot analysis of HCT116 WT and DN-PKcs null cells. Cells were incubated in normoxia (N) and hypoxia (H) for 4 hrs followed by lysis. Whole cell lysates were then subjected to Westernblot analysis for HIF-1α and actin. **B:** HCT116 and DNA-PKcs-/- cells were subjected to 4 hrs of hypoxia followed by reoxygenation for indicated times and then subjected to WB analysis for HIF-1α and and Ku80

Exp 2: DNA-PKcs inhibitor Nu7441 attenuates HIF-1α induction upon hypoxia. HCT116 cells were pretreated with DNA-PKcs kinase inhibitor Nu7441 (10 and 20 μM, for 1hr), and were subjected to 4 hrs of hypoxia alone (H) or additional 20 min of reoxygenation (H+Oxy). Whole cell lysates were subjected to western blot analysis. The result showed that increasing dosages of DNA-PKcs kinase inhibitor Nu7441 correlates to the attenuated HIF-1α stabilization in response to hypoxia. This result thus demonstrated that kinase activity of DNA-PKcs is required for HIF-1α stabilization in response hypoxic environment

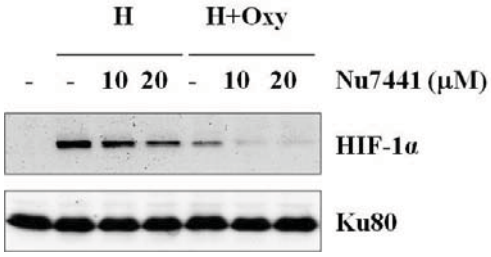

Exp 2: HCT116 cells were pretreated with DNA-PKcs kinase inhibitor Nu7441 (10 and 20 μM, for 1hr), and were subjected to 4 hrs of hypoxia alone (H) or additional 20 min of reoxygenation (H+Oxy). Whole cell lysates were subjected to WB analysis for HIF-1α and Ku80.

Exp 3: DNA-PKcs inhibitor Nu7441 attenuates HIF-1α induction upon hypoxia. HCT116 cells were pretreated with DNA-PKcs kinase inhibitor Nu7441 (10 and 20 μM , for 1hr), and were subjected to 4 hrs of hypoxia alone or followed by reoxygenation for 20 or 60 min. Whole cell lysates were analyzed in western blot as indicated. The result confirmed our studies that: i) DNA-PKcs is required for hypoxia-induced HIF-1α, lane #2-4 vs #12-14, and ii) DNA-PKcs inhibitor Nu7441 attenuates hypoxia-induced HIF-1α stabilization, lane #2 vs #3/4. In addition, we observed differential regulation of Akt Ser308 phosphorylation (by PDK-1 kinase?) in HCT116 and PKcs-/- cells upon hypoxia/reoxygenation. Increase of Akt Ser308 phosphorylation was observed in HCT116 cells only after reoxygenation (lane #5 vs #2), whereas it was significantly induced in DNA-PKcs -/- cells upon hypoxia (lane #12 vs #11) and reoxygenation did not further increase the level of Akt phosphorylation. Our results suggest that DNA-PKcs participates not only HIF-1α stabilization upon hypoxia but also is required for and normal cellular response/regulation of oxidative stress.

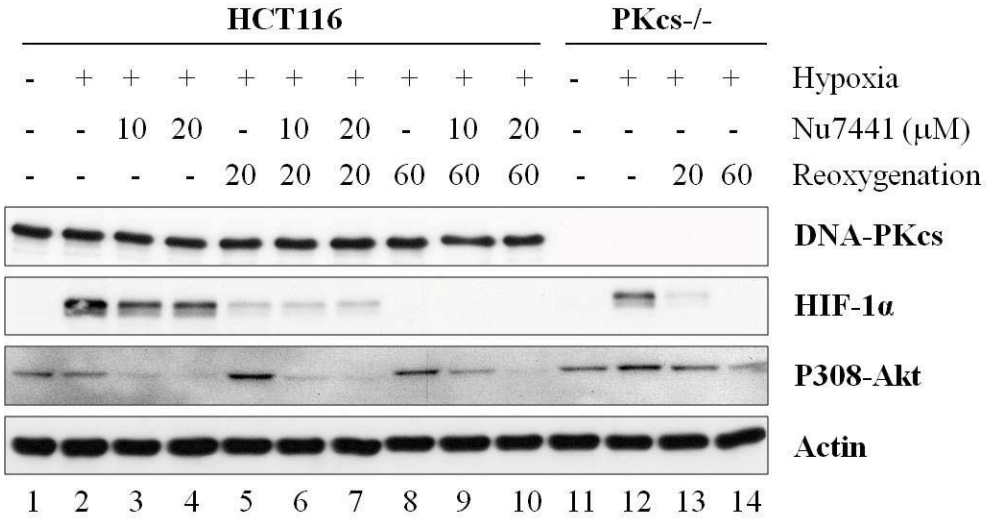

Exp 3: HCT116 WT and DNAPKce null cells were pretreated with DNA-PKcs kinase inhibitor Nu7441 (10 and 20 μM for 1hr), and were subjected to 4 hrs of hypoxia alone or followed by reoxygenation for 20 or 60 min. Whole cell lysates were analyzed in western blot as indicated for DNA-PKcs, HIF-1α, p308-Akt and Actin.

Exp 4: Role of DNA-PKcs on HIF-1α expression in DAB2IP deficient or proficient prostate cancer cells. For this study, we used prostate cancer (PCa) cell lines C4-2 Neo (DAB2IP deficient) and C4-2D2 (DAB2IP proficient) cell lines. First we check the DNA-PKcs and HIF-1α level in these two cell lines under normoxia (N) and hypoxia (H). As shown in the following figure, HIF-1α induction was noticed under hypoxia in both cell lines however, no significant difference in DNA-PKcs expressing was noticed in +/- DAB2P protein (Panel **A**). This result was significantly different when compare to human colon cancer cell as shown in Exp: 1A where the expression of HIF-1α under hypoxia was undetectable in the absence of DNA-PKcs. DAB2IP expression in C4-2D2 cells was not changed under N or H condition. We also tested several phospho-rylation sites on DNA-PKcs; interestingly, the basal phosphorylation of both Ser2056 and Thr2609 is higher in DAB2IP over-expressed cell lines (C42-D2) which we will investigate in the future (Panel **A**). In summary, DNA-PKcs regulates HIF-1α differently in human colon and prostate cell lines. To further investigate the role of DNA-PKcs we treated PCa cells with an inhibitor of DNA-PKcs, NU7441 under hypoxia. As shown in the following figure we observed no change in HIF-α level in +/- NU7441 indicating that DNA-PKcs is probably not involved in HIF-1α stabilization in PCa cells (Panel **B**).

In another study, both C4-2 neo and C4-2D2 cells were co-transfected with 5XHRE-Luc reporter and renilla luciferase (for internal control) followed by 5 μM NU7441 and hypoxia treatment for 16 hrs, then dual luciferase reporter assay was performed. At the same time, the cell lysates were collocated

from a separate experiment and subjected to western blot analysis with the antibodies against HIF-1α and actin. As shown in the following figure (panel **C**), HIF-1α induced in both cell lines under hypoxia and the addition of NU7441 did not affect the HIF-1α stability. Luciferase activity (panel D) also significantly enhanced in both cell lines in hypoxia and no effect of NU7441 on HIF-1α activity was noticed.

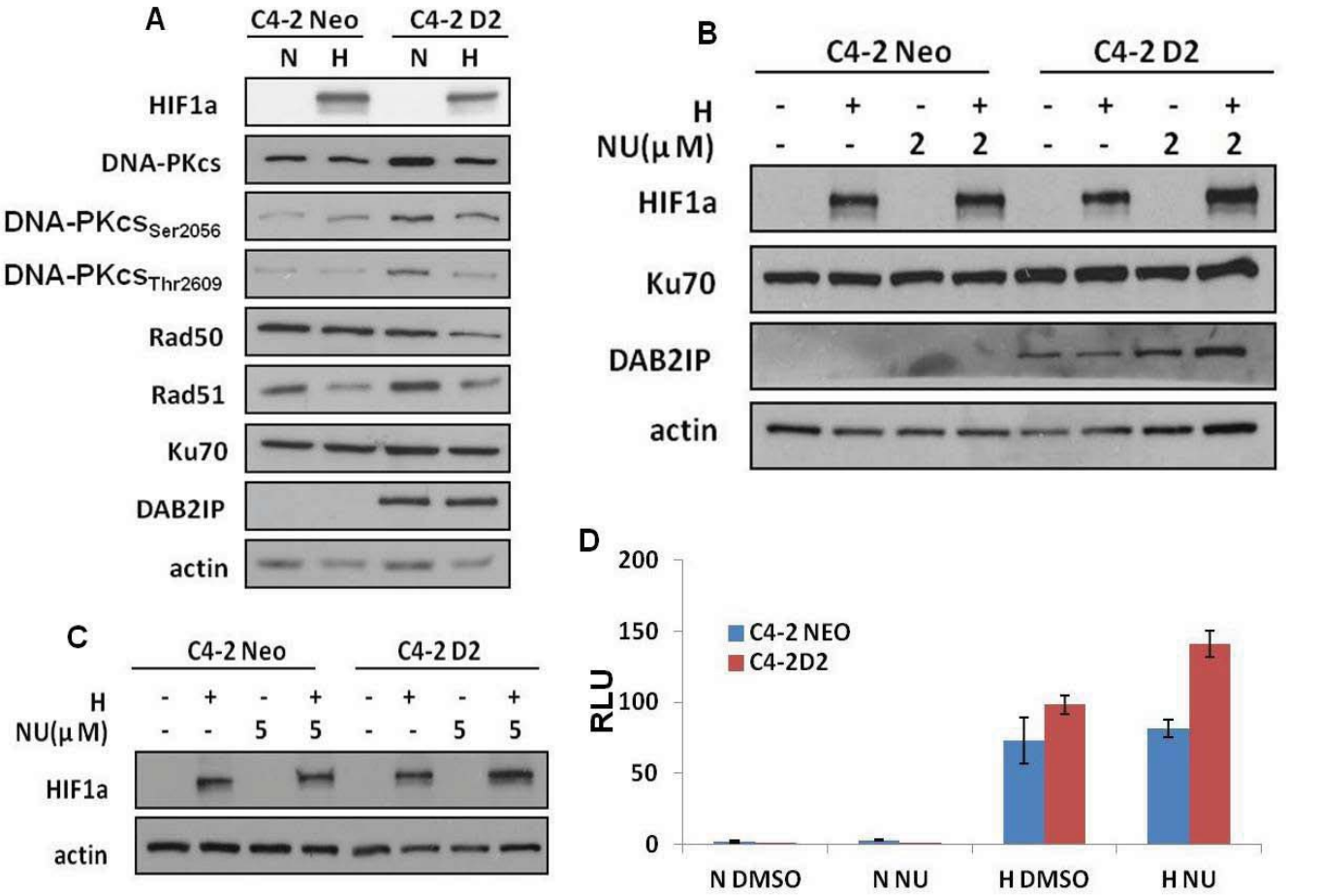

Exp 4: A: C4-2 Neo (DAB2IP deficient) and C4-2D2 (DAB2IP proficient) cell lines were treated as indicated in normoxia (N) and hypoxia (H) and then subjected to WB analysis for various proteins as shown. **B-C**: WB analysis of HIF-1a in PCa cells in after treatment with Nu7441 as indicated. D: C4-2 neo and C4-2D2 cells were co-transfected with 5XHRE-Luc reporter and renilla luciferase (for internal control) followed by 5 μM NU7441 and hypoxia treatment for 16 hrs, then dual luciferase reporter assay was performed.

Task 7:

Exp 1: Our original finding of DNA-PKcs's role on HIF-1α stability under hypoxic condition was observed in HCT116 cells, therefore, we proposed to perform similar studies in prostate cancer cells after knocking down DNA-PKcs. However, our results in C4-2 Neo and C4-2 D2 cells showed that the stability of HIF-1α is not completely dependent on DNA-PKcs. As shown above, that in multiple experiments using specific DNA-PKcs inhibitors, we were unable to demonstrate HIF- 1α destabilization as we have seen in HCT116 cells. Therefore, the mechanism of HIF-1α regulation is different in various cancer types. We also studied in other PCa cell lines (PC3 and DU145) but no appreciable change was noticed. We perform luciferase assays as proposed in Task 7 and the results were shown in previous section. Therefore, to perform further experiments as proposed in task 7 will not be helpful.

Interestingly, while studying the regulation of HIF-1α in PCa cells, we noticed that in different cell cycle phases the human DAB2IP protein was often detected as doublet. As shown in the following panels (A and B). We then found that upper band of DAB2IP disappeared when the mitotic cell lysates were treated with lambda protein phosphatase (λ-PPase) (Panel C). These results indicated that DAB2IP could be phosphorylated during mitosis. Next, we examined the kinetics of DAB2IP phosphorylation during the cell cycle. Phosphorylation of DAB2IP peaked at 16-18 h after the release from thymidine release, when most cells entered mitosis (Panel D). Furthermore, when the cells exited mitosis, DAB2IP was rapidly dephosphorylated (Panel E).

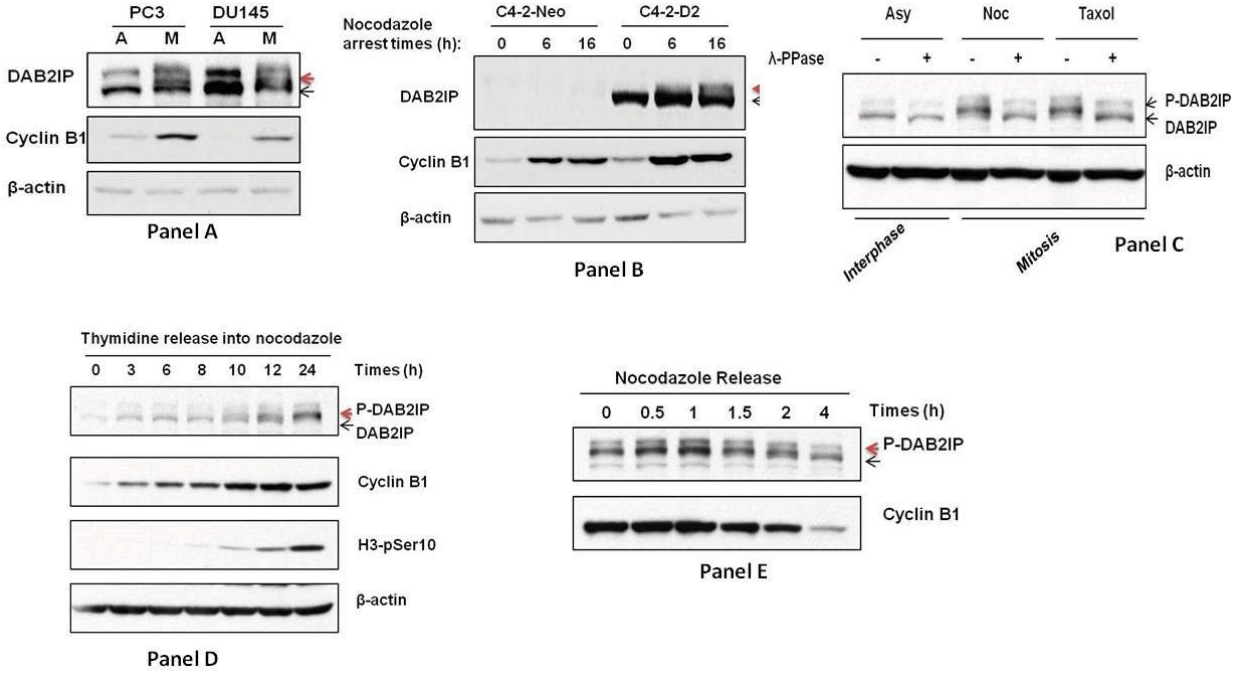

Exp 1: DAB2IP could be phosphorylated during mitosis. **(A)** Asynchronous (A) and nocodazole-arrested (M) extracts from PC3 and DU145 cells were performed immunoblotting with antibodies against DAB2IP, cyclin B1 and actin. **(B)** Asynchronous and nocodazole-arrested extracts from DAB2IP overexpressed C4-2 cells were performed immunoblotting with antibodies against DAB2IP, cyclin B1 and actin. **(C)** Asynchronous (Asy.) and nocodazole-arrested (Noc.), paclitaxel-arrested (Taxol.) extracts from PC3 cells were treated with/without λ-PPase, followed by immunoblotting with antibodies against DAB2IP, cyclin B1 and actin. **(D)** PC-3 cells were synchronized by a double thymidine treatment and then released into nocodazole. Cell extracts were prepared at the indicated times after nocodazole treatment. Immunoblot analysis was carried out using the indicated antibodies. **(E)** Nocodazole-arrested PC3 cells were collected by shake-off and then released into fresh media. The samples were collected at the times as indicated and were subjected to western blot analysis.

Exp 2: Next we are looking for possible kinases that can phosphorate DAB2IP. It is known that Cdk1 kinase plays dominant role in G2-M transition. We tested whether DAB2IP was one of Cdk1 substrates by using an inhibitor of Cdk 1 AZD5438. The result shows that AZD5438 abolished the phosphorylation of DAB2IP in mitotic lysates (Panel A). We also knocked down the Cdk1 using specific siRNA and the knockdown Cdk1 also prevented the phosphorylation of DAB2IP in mitosis (Panel B). We further immunoprecipitated DAB2IP from nocodazole arrested C4-2 D2 cells and then performed western blotting to detect the phosphorylation signal using anti-Cdks mediated Ser and Thr phosphorylation antibodies. We found that both of these antibodies can recognize phosphorylated DAB2IP (Panel C). This result indicated that DAB2IP can be phosphorylated both at Ser and Thr sites during mitosis.

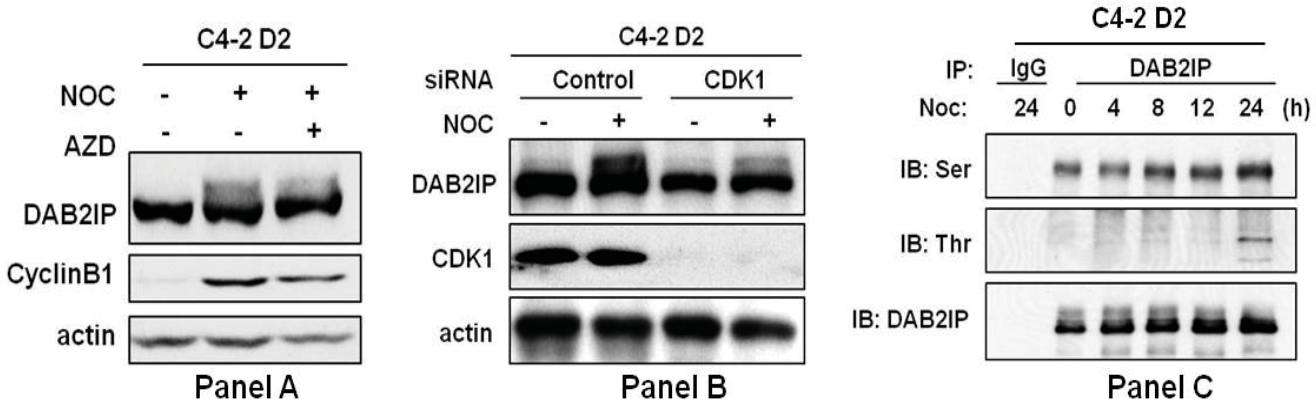

Exp 2: DAB2IP could be phosphorylated by CDK1 during mitosis**. (A)** C4-2 D2 cells were treated with Nocodazole (50ng/ml) for 12 hours followed by AZD5438 (500nM), samples were collected at 4 hours and analysed by western blot**. (B)** C4-2 D2 cells were transfected with Cdk1-specific siRNAs (200 pmol) or scrambled siRNAs (200 pmol). After 24 hours, cells were treated with Nocodazole (50ng/ml) for 16 hours and the samples were subjected to western blot analysis. **(C)** C4-2 D2 cells were treated with Nocodazole (50ng/ml), cell lysates were collected at indicated times and immunoprecipitated (IP) with an anti-DAB2IP antibody or normal rabbit IgG and then the immunoprecipitates were analysed by western blot with anti-Cdks mediated Ser and Thr phosphorylation antibodies and anti-DAB2IP antibody.

Exp 3: With these observations, we then investigated the role of DAB2IP in mitotic cells. A significant increase in metaphase cells and decrease in anaphase cells were found in the DAB2IP overexpressed C4-2 D2 cells relative to control cells (C4-2 Neo) which suggests a robust spindle checkpoint in mitotic cells (Panel A and B). To determine the effect of the DAB2IP on spindle assemble checkpoint, C4-2D2 and C4-2 Neo cells were treated with 50ng/ml nocodazole and harvest at different time points for analysis. We found that the C4-2 D2 cells arrested better than control cells. By 24h, more that 60% cells arrested at mitosis in C4-2 D2 cells, whereas

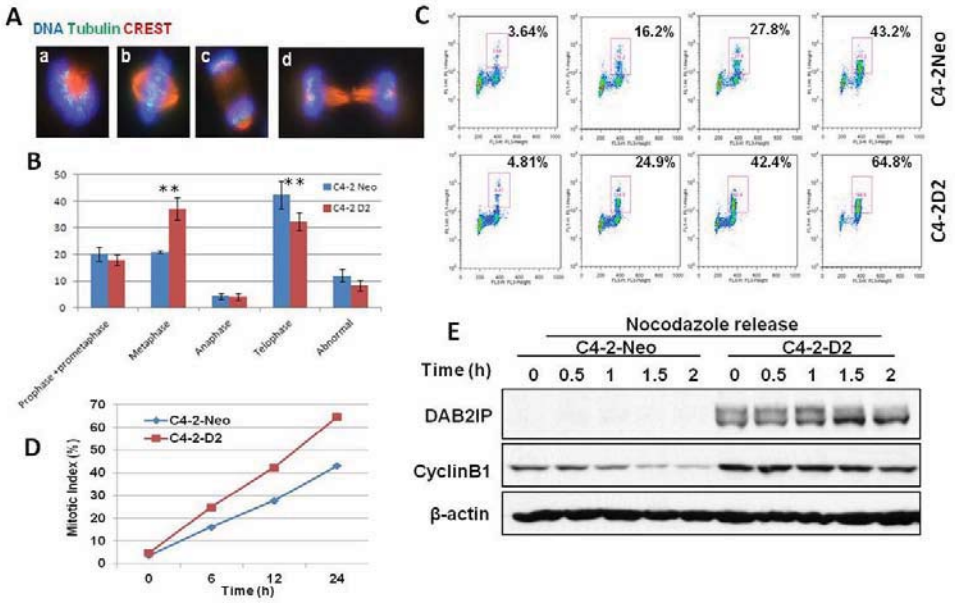

Exp 3: DAB2IP regulated SAC. **(A)** Unperturbed DAB2IP overexpressed C4-2 cells and control cells undergoing mitosis were stained for tubulin (red), crest (green) and DAPI (blue). a, prometaphase; b, metaphase; c, anaphase; d, telophase. **(B)** Percentage distribution (mean ± SE) of cells in different phases of mitosis and cytokinesis was analyzed. **(C)** DAB2IP overexpressed C4-2 cells were treated with Nocodazole (50ng/mL) for the indicated time and stained with propidium iodide and anti-pS10-histone H3 (pH3) antibody and were analyzed by flow cytometry. **(D)** Quantification of the mitotic index. **(E)** DAB2IP overexpressed C4-2 cells and control cells were synchronized at prometaphase by a nocodazole (Noc.) arrest. Mitotic cells were collected by shake-off, released into fresh medium and then collected at the indicated times after release. Levels of cyclin B1, DAB2IP and actin were determined by western blot analysis.

only 40% in control cells (Panel C and D). To directly test whether DAB2IP was required for checkpoint activation, we examined the degradation kinetics of cyclin B1 in C4-2 cells after releasing from nocodazole arrest. When compared with control cells, cyclin B1 were markedly stabilized in C4-2 D2 cells (Panel E). These results suggest that DAB2IP might be required for the release of checkpoint inhibition of APC/C and probably functions downstream of the kinetochore pathway.

Task 8:
Currently we are preparing the manuscripts using the results as described above. The manuscript will be submitted in a peer reviewed journal.

Task 9:
We have also initiated our studies as described in Task 9. We have already standardized the conditions to develop prostate orthotopic model in rodents (Rats). We are monitoring the tumor growth using different imaging modalities including bioluminescence (BLI), ultrasound and MRI. We have also performed image guided radiation treatment to these prostate tumors and then follow up the tumor progression using BLI. Our next experiments will be the combination of Radiation and Nu7441 in treating these rats with prostate tumors and also monitor the normal tissue toxicity to the surrounding organ as proposed in the original proposal. A part of our ongoing study is now published in the ***Journal of International of Oncology*** and the copy of this article is attached with report.

Reportable outcomes

As mentioned earlier, we have published two articles;

1. DAB2IP regulates autophagy in prostate cancer in response to combined treatment of radiation and a DNA-PKcs inhibitor (20123). Lan Yu, Vasu Tumati, Shu-Fen Tseng, Feng-Ming Hsu, D. Nathan Kim, David Hong, Jer-Tsong Hsieh, Corbin Jacobs, Payal Kapur and Debabrata Saha; *Neoplasia*, **14**, 1203–1212

2. Development of a locally advanced orthotopic prostate tumor model in rats for assessment of combined modality therapy (2013). Vasu Tumati, Sanjeev Mathur, Kwang Song, Jer-Tsong Hsieh, Dawen Zhao, Masaya Takahashi, Timothy Dobin, Leah Gandee, Timothy D. Solberg, Amyn A. Habib and Debabrata Saha; *International Journal of Oncology*, **42**, 1613-1619

In addition, Lan Yu also presented the Poster in the American Association of Cancer research Meeting held in Chicago, 2012

Conclusion:
We have made significant progress which we described under Task 5, 6, 7 and 9. We are highly hopeful to finish the remaining tasks in appropriate time.

References: References are included in the attached manuscript

Appendices:
Published articles by Yu *et al* and Tumati *et al* are attached.

NEOPLASIA
www.neoplasia.com

Volume 14 Number 12 December 2012 pp. 1203–1212 1203

DAB2IP Regulates Autophagy in Prostate Cancer in Response to Combined Treatment of Radiation and a DNA-PKcs Inhibitor[1,2]

Lan Yu*, Vasu Tumati*, Shu-Fen Tseng†, Feng-Ming Hsu‡, D. Nathan Kim*, David Hong*, Jer-Tsong Hsieh§,¶, Corbin Jacobs*, Payal Kapur# and Debabrata Saha*,¶

*Department of Radiation Oncology, University of Texas Southwestern Medical Center, Dallas, TX; †Department of Bioengineering, University of Texas at Arlington, Arlington, TX; ‡Department of Oncology, National Taiwan University Hospital, National Taiwan University College of Medicine, Taipei, Taiwan; §Department of Urology, University of Texas Southwestern Medical Center, Dallas, TX; ¶Simmons Comprehensive Cancer Center, Dallas, TX; #Department of Pathology, University of Texas Southwestern Medical Center, Dallas, TX

Abstract

Radiation therapy (RT) is an effective strategy for the treatment of localized prostate cancer (PCa) as well as local invasion. However, some locally advanced cancers develop radiation resistance and recur after therapy; therefore, the development of radiation-sensitizing compounds is essential for treatment of these tumors. DOC-2/DAB2 interactive protein (DAB2IP), which is a novel member of the Ras–GTPase activating protein family and a regulator of phosphatidylinositol 3-kinase–Akt activity, is often downregulated in aggressive PCa. Our previous studies have shown that loss of DAB2IP results in radioresistance in PCa cells primarily because of accelerated DNA double-strand break (DSB) repair kinetics, robust G_2/M checkpoint control, and evasion of apoptosis. A novel DNA-PKcs inhibitor NU7441 can significantly enhance the effect of radiation in DAB2IP-deficient PCa cells. This enhanced radiation sensitivity after NU7441 treatment is primarily due to delayed DNA DSB repair. More significantly, we found that DAB2IP-deficient PCa cells show dramatic induction of autophagy after treatment with radiation and NU7441. However, restoring DAB2IP expression in PCa cells resulted in decreased autophagy-associated proteins, such as LC3B and Beclin 1, as well as decreased phosphorylation of S6K and mammalian target of rapamycin (mTOR). Furthermore, the presence of DAB2IP in PCa cells can lead to more apoptosis in response to combined treatment of NU7441 and ionizing radiation. Taken together, NU7441 is a potent radiosensitizer in aggressive PCa cells and DAB2IP plays a critical role in enhancing PCa cell death after combined treatment with NU7441 and radiation.

Neoplasia (2012) 14, 1203–1212

Abbreviations: PCa, prostate cancer; DAB2IP, DOC-2/DAB2 interactive protein; mTOR, mammalian target of rapamycin; IR, ionizing radiation; RT, radiation therapy; DSBs,double-strand breaks; 6-TG, 6-thioguanine; BRFS, biochemical recurrence-free survival; IHC, immunohistochemistry; AVOs, acidic vesicular organelles

Address all correspondence to: Debabrata Saha, PhD, Department of Radiation Oncology, Division of Molecular Radiation Biology, University of Texas Southwestern Medical Center, 2201 Inwood Road, Dallas, TX 75390-9187. E-mail: debabrata.saha@utsouthwestern.edu

[1]This work was supported by the funding from Department of Defense Idea Award W81XWH-11-1-0270 (D.S.), Flight Attendant Medical Research Institute Award grant (D.S.), and a Clinical Research Fellowship (V.T.) from the Doris Duke Charitable Foundation. Conflict of interest: None.
[2]This article refers to supplementary material, which is designated by Figure W1 and is available online at www.neoplasia.com.
Received 8 August 2012; Revised 10 October 2012; Accepted 12 October 2012

DOI 10.1593/neo.121310

Introduction

Prostate cancer (PCa) is the most common type of non-skin cancer and the second leading cause of cancer-related death in U.S. men [1]. Radiation therapy (RT) provides excellent local control and increased overall survival for PCa [2]. However, a significant proportion of high-risk patients display radiation resistance and develop metastatic disease in less than 5 years [3]. Elucidation of biomarkers and their effects on mediating therapeutic resistance may allow physicians to personalize care based on genotype. DOC-2/DAB2 interactive protein (DAB2IP)/AIP1, a novel member of the RAS–GTPase activating protein family, acts as a tumor suppressor but is often downregulated in aggressive PCa [4]. Our previous work demonstrated that loss of DAB2IP expression results in increased radioresistance in both PCa cells and normal prostate epithelia [5,6]. Therefore, elucidating the mechanism by which loss of DAB2IP induces radioresistance will provide useful information in identifying new strategies to sensitize DAB2IP-deficient PCa cells to RT.

DNA-PKcs, the catalytic subunit of DNA-dependent protein kinase and member of the phosphatidylinositol 3-kinase (PI3K)–like family, plays a dominant role in nonhomologous end joining (NHEJ)–mediated DNA double-strand break (DSB) repair [7]. Furthermore, DNA-PKcs may play a role in initiating DNA DSB–induced apoptosis [8,9]. Upon recruitment to DSB sites, DNA-PKcs phosphorylates downstream targets involved in DNA repair response and promotes direct ligation of broken DNA ends. Accordingly, suppression of DNA-PKcs leads to ineffective DSB repair and increases the cytotoxicity of ionizing radiation (IR) and other DSB-inducing agents [10]. On the basis of the important role of DNA-PKcs in NHEJ, inhibition of DNA-PKcs is, therefore, an attractive approach to overcome the resistance of RT. Our primary goal of this study is to develop strategies to overcome radioresistance of DAB2IP-negative PCa and improve the efficacy of RT in PCa using NU7441, a potent and specific inhibitor of DNA-PKcs.

Recent studies suggest that DNA-PKcs is involved in DNA damage–induced autophagy. Specifically, inhibition of DNA-PKcs sensitized malignant glioma cells to radiation-induced autophagic cell death [11]. However, autophagy, which normally results in degradation of damaged or potentially dangerous proteins and organelles, may have a pro-survival function, which protects cells from various forms of cellular stress [12]. Several studies indicate that pharmacologic or genetic inhibition of autophagy can enhance cancer treatments by sensitizing cancer cells to both radiation and chemotherapy [13]. On the basis of these reports, we analyzed the levels of autophagy in NU7441-treated DAB2IP-deficient and DAB2IP-proficient PCa cells to investigate whether suppression of DNA-PKcs can confer to radiation-induced autophagy in PCa cells. In this study, we show a novel function of DAB2IP in suppressing IR-induced and DNA-PKcs–associated autophagy and promoting apoptosis in PCa cells. Despite that NU7441 could significantly enhance the effect of RT in DAB2IP-negative PCa, the combination of NU7441 and DAB2IP expression resulted in greater RT efficacy due to autophagy inhibition.

Materials and Methods

Cell Culture and Irradiation

PCa cell lines C4-2 and PC3 were grown in T medium (Invitrogen, Carlsbad, CA) with 5% FBS (HyClone, Hudson, NH) at 37°C with 5% CO_2 in a humidified chamber. C4-2 neo (DAB2IP-negative) and C4-2 D2 (DAB2IP-positive) were generated from C4-2 cells, and PC3 Con (DAB2IP-positive) and PC3 KD (DAB2IP knockdown) were generated from PC3 cells as described previously [5]. All cells were irradiated in ambient air using a ^{137}Cs source (Mark 1-68 irradiator; J.L. Shepherd & Associates, San Fernando, CA) at a dose rate of 3.47 Gy/min at room temperature. NU7441 was purchased from Tocris Bioscience (Ellisville, MO); NVP-BEZ225 was purchased from SelleckBio (Houston, TX); rapamycin and RAD001 (Everolimus) were purchased from LC Laboratories (Woburn, MA); LY294002 was purchased from EMD Millipore (Billerica, MA).

Antibodies

Anti–phospho-histone γH2AX (Ser^{139}) was obtained from EMD Millipore. 53BP1, mammalian target of rapamycin (mTOR), phospho-mTOR (pmTOR, S2448), phospho-S6 kinase (pS6K, T389), AKT, phospho-AKT (pAKT, S473), LC3B, Beclin 1, and poly (ADP-ribose) polymerase (PARP) antibodies were purchased from Cell Signaling Technology (Danvers, MA). Anti-actin antibody was purchased from Sigma-Aldrich (St Louis, MO). Fluorescent dye–conjugated secondary antibodies were obtained from Invitrogen.

Clonogenic Survival Assay

Exponentially growing cells were trypsinized and counted using a Coulter counter (Beckman Coulter, Fullerton, CA). Cells were diluted serially to appropriate concentrations and plated into 60-mm dishes in triplicates. After 3 hours of incubation, cells were treated with increasing doses of IR (2, 4, 6, and 8 Gy) or NU7441 (1 μM) or NU7441 + IR. After 10 to 14 days, cells were fixed and stained with 4% formaldehyde and 0.05% crystal violet in phosphate-buffered saline (PBS). Colonies containing >50 cells were counted. Surviving fraction (SF) was calculated as (mean colony counts)/[(cells inoculated) × (plating efficiency)], in which plating efficiency was defined as (mean colony counts)/(cells inoculated for unirradiated controls). The data are presented as the mean ± SD of at least three independent experiments. The curve $S = e^{-(\alpha D + \beta D2)}$ was fitted to the experimental data with a least-squares fit algorithm using the program Sigma Plot 11.0 (Systat Software, Inc, Chicago, IL).

The Detection of γH2AX and 53BP1 Foci

The 53BP1 and phosphorylation of H2AX (γH2AX) were used as an indicator of DNA DSB. Cells were cultured for the indicated times to repair DNA lesions after irradiation either alone or combined with NU7441. The cells were fixed in 4% paraformaldehyde/PBS for 30 minutes, permeabilized in 0.5% Triton X-100/PBS for 15 minutes, and blocked in 5% BSA for 30 minutes. The samples were incubated with anti–phospho-histone γH2AX (Ser^{139}; 1:2000) and 53BP1 (1:500) for 1 hour, washed in PBS for 10 minutes three times, and incubated with Alexa Fluor 488–conjugated goat anti-rabbit and rhodamine red–conjugated goat anti-mouse secondary antibodies (1:1000) for 1 hour. The cells were washed for 10 minutes three times and mounted using VECTASHIELD mounting medium with 4′,6-diamidino-2-phenylindole (DAPI; Vector Laboratories, Burlingame, CA). The number of γH2AX and 53BP1 foci was examined using a fluorescence microscope.

Cell Cycle Analysis

The treatment or control cells were harvested and fixed using 75% ethanol either immediately or at the indicated time after radiation and radiation + NU7441. The cells were resuspended in PBS containing 1 μg/ml RNase A (Sigma, St Louis, MO), incubated for 30 minutes at 37°C, and stained with 100 μg/ml propidium iodide (Sigma)

for 15 minutes at 4°C. The cell cycle distribution was analyzed using flow cytometry, and a minimum of 10,000 cells per sample were counted.

Detection of Acidic Vesicular Organelles

Cells were grown in 60-mm dishes and allowed to attach overnight. The cells were treated with radiation or radiation + NU7441 as indicated and then were incubated with 1 μg/ml acridine orange (AO)/PBS for 15 minutes, washed with PBS, and examined under LSM 510 laser scanning confocal microscope (Zeiss) at ×63 magnification. Untreated cells were also cultured for 3 days as a negative control. The samples were collected for FACScan and analyzed using Flowjo 8.7.1 (Tree Star, Inc, Ashland, OR) software to quantify cells that were positive for acidic vesicular organelles (AVOs).

Retrospective Cohort Analysis

Patients with high-risk disease (stage T3a or greater, Gleason score > 7, or prostate-specific antigen > 20) treated with definitive RT between 2005 and 2011 at the University of Texas Southwestern Medical Center were identified. Immunohistochemistry (IHC) analysis for DAB2IP protein was performed on their biopsy specimens. DAB2IP status was scored in the tumors by an expert genitourinary pathologist. A loss of DAB2IP was determined by one or more biopsy cores with decreased expression of the protein in the prostatic adenocarcinoma compared to the surrounding normal prostate tissue. Biochemical recurrence-free survival (BRFS) of patient cohorts with and without DAB2IP loss was determined using the Phoenix definition. Log-rank test was used to correlate BRFS with DAB2IP levels. Univariate analysis of BRFS to pretreatment prostate-specific antigen, Gleason score, stage, age, and DAB2IP status was performed.

Statistical Analysis

Data are presented as the means ± SD of at least three independent experiments. The results were tested for significance using the unpaired Student's *t* test.

Results

NU7441 Sensitizes DAB2IP-deficient Cells to Irradiation

To test the effect of NU7441 on the radiosensitivity of DAB2IP-positive and DAB2IP-negative PCa cells, we employed PC3 cell line (DAB2IP-positive) and C4-2 cell line (DAB2IP-negative) and its

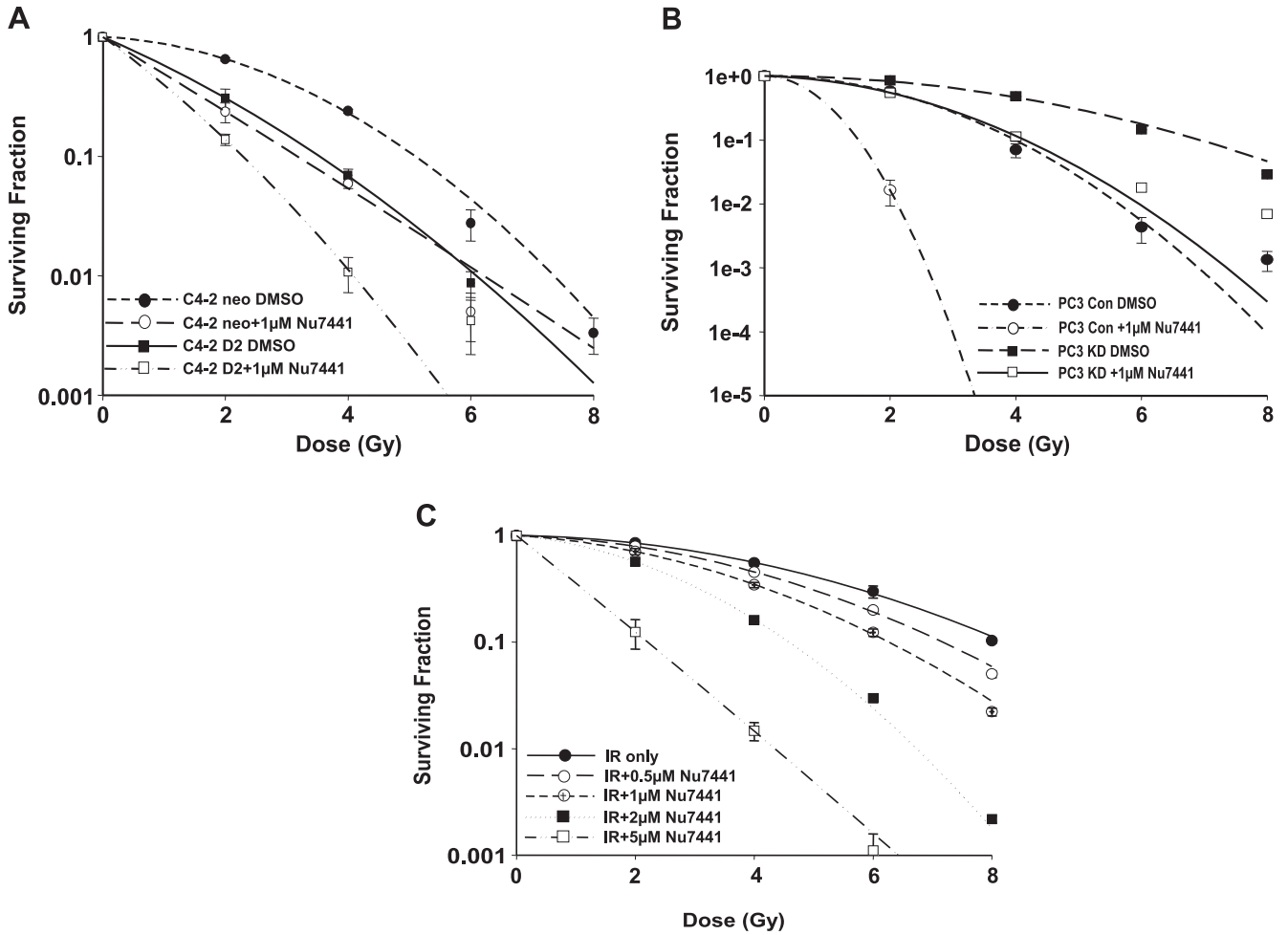

Figure 1. NU7441 increases the radiosensitivity in both DAB2IP-negative and DAB2IP-positive PCa cell lines. (A) The SF analysis of C4-2 D2 and C4-2 neo cells after combined treatment with 1 μM NU7441 and IR as indicated. (B) SF analysis of DAB2IP-knockdown PC3 cells (PC3-KD) and PC3 Con cells after treatment with 1 μM NU7441 and IR as indicated. (C) The survival curves of PC3 KD cells after combination treatment with 0.5 to 5 μM NU7441 and irradiation at doses of 0 to 8 Gy. In all studies, results are expressed as the means ± SD from three independent experiments.

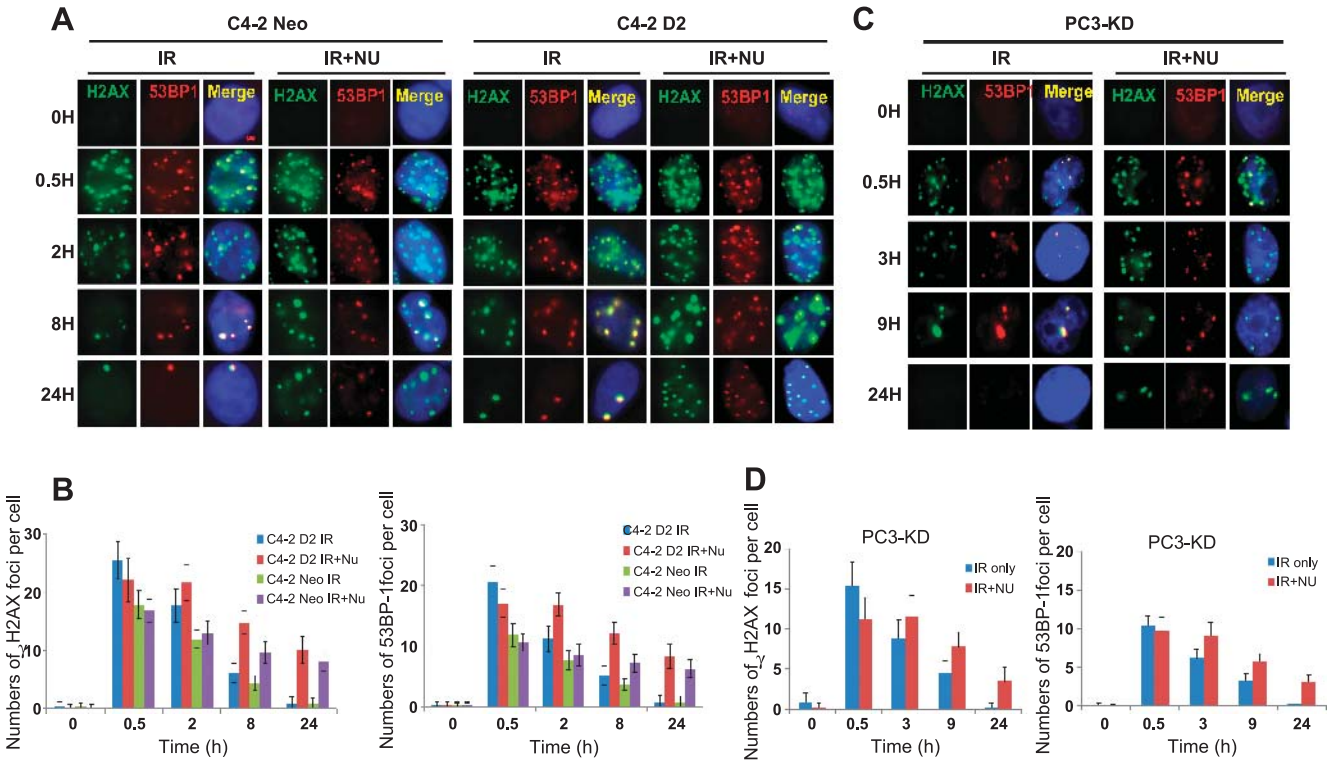

Figure 2. NU7441 blocks IR-induced DNA DSB repair in DAB2IP-positive and DAB2IP-negative PCa cells. PCa cells were treated with 2 μM NU7441 for 30 minutes followed by IR (2 Gy); samples were collected at the indicated time points after IR, immune-stained for 53BP1 (red foci) and phospho-γH2AX (green foci), and counted (average, 50 nuclei). (A) C4-2 D2 and C4-2 neo cells. (B) PC3-KD cells. Quantitative analysis of DNA repair kinetics between C4-2 cells (C) and PC3KD cells (D).

sublines [5]. As shown in Figure 1, *A* and *B*, DAB2IP-specific shRNA-mediated suppression of endogenous DAB2IP significantly increased radiation resistance in PC3 cells (Figure 1*B*). In contrast, the presence of DAB2IP resulted in a significant radiation-sensitizing effect in C4-2 D2 cells (Figure 1*A*). Using colony formation assays, we found that NU7441 significantly sensitized DAB2IP-negative (C4-2 neo and PC3-KD) cells to IR. SF at 2 Gy (SF_2) for C4-2 neo and PC3 KD cells was reduced from 0.65 ± 0.023 and 0.86 ± 0.04 to 0.24 ± 0.04 and 0.55 ± 0.06, respectively. Here, we confirm, as previously shown [5], that DAB2IP-expressing cells are more radiosensitive when compared to DAB2IP-deficient cells. Furthermore, we found that NU7441 further sensitized DAB2IP-proficient cells to IR. SF_2 values of C4-2 D2 and PC3 Con vector cells were decreased from 0.31 ± 0.06 and 0.58 ± 0.06 to 0.14 ± 0.02 and 0.02 ± 0.007, respectively. The radiation-sensitizing effect of NU7441 is dose dependant (Figure 1*C*). These *in vitro* results indicate that NU7441 can radiosensitize both DAB2IP-positive and DAB2IP-negative PCa cells to radiation.

NU7441 Blocks IR-Induced DNA DSB Repair in DAB2IP-Positive and DAB2IP-Negative PCa Cells

The extent of DNA DSBs generated and the ability of tumor cells to repair the damage largely determine the efficacy of RT. Therefore, to investigate whether the radiosensitizing effect of NU7441 on DAB2IP-deficient cells was a result of compromised DSB repair, we subjected cells to immunofluorescence staining for phosphorylated histone H2AX (γH2AX) (green) and 53BP1 (red) (Figure 2, *A* and *C*) and determined DNA DSB repair kinetics by counting the separate foci at each time point. In this study, C4-2 neo and D2 cells were exposed to 2 μM NU7441 for 1 hour before 2-Gy IR treatment and the cells were collected at various times as indicated. As shown in Figure 2*C*, rapid induction of DNA damage was detected within 30 minutes in all of the cells. In untreated cells, DNA DSB foci were almost abolished at 24 hours after IR, whereas a significant number of DSBs remained at 24 hours in NU7441-treated cells; similar results were present in PC3-KD cells (Figure 2, *B* and *D*). The residual number of DSB foci per nucleus in DAB2IP-expressing C4-2 cells was significantly higher than the control cells 30 minutes after IR; however, detectable foci fell to the same level as control cells 24 hours after IR. This result indicates that the presence of DAB2IP in C4-2 cells promotes IR-induced DNA DSBs but has no effect on repair kinetics. Taken together, these results show that NU7441 can lead to defective DNA damage repair in response to IR even in DAB2IP-deficient metastatic PCa cells.

In mammalian cells, IR-induced cell cycle arrest is necessary to maintain genomic stability and is correlated to cell survival. In this study, the effect of NU7441 on cell cycle distribution was investigated by flow cytometry. As shown in Figure 3, *A* to *D*, treatment with 2 μM NU7441 resulted in robust G_2/M arrest 24 hours after irradiation (2 Gy) in both DAB2IP-deficient or DAB2IP-expressing cell lines. We further compared C4-2 neo and D2 cells and showed that the percentage of G_0/G_1 phase cells in C4-2 D2 was more than that in neo (control) line. The cell cycle results indicate that DAB2IP alone causes significant G_0/G_1 arrest in C4-2 cells and is augmented after treatment with either IR or NU7441, whereas DAB2IP-deficient cells showed moderate increase in G_0/G_1 arrest after NU7441 treatment. However, both cell lines showed robust G_2/M arrest at 24 hours in response to combined treatment.

DAB2IP Inhibits Irradiation-induced Autophagy

Autophagy is the mechanism of proteolysis and has been involved in both cell survival and cell death [14]. In general, autophagy protects cells from stressful conditions such as nutrient deprivation. There are reports also indicating that autophagy protects cells from radiation [15]. To test whether DAB2IP is involved in PCa cell autophagy, first we analyzed the formation of AVOs using AO staining with fluorescence imaging and flow cytometry. During autophagy, AO accumulates in acidic compartments such as autolysosomes. Using a laser scanning confocal microscope, we found that the autophagic signal increases in DAB2IP-deficient C4-2 neo cells after IR, NU7441, and the combination of NU7441 and IR treatment. However, across the all three treatment arms, there was a significant decrease in the amount of autophagy in the DAB2IP-expressing cell line C4-2 D2 (Figure 4*A*). To further confirm this result, we performed flow cytometric analyses of AO-stained cells. As shown in Figure 4*B*, DAB2IP-deficient cells display significantly more autophagy than DAB2IP-expressing cells. We also performed the immunostaining with LC3B antibody (Figure 4*C*) and the results were consistent with Figure 4, *A* and *B*. We further subjected C4-2 neo cells to IR combined with an autophagy inhibitor, Bafliomycin A1 (Baf A1). The clonogenic assay clearly showed that Baf A1 treatment enhanced radiation-induced cell death in DAB2IP-deficient PCa cells (Figure 4*D*). On the basis of these results, we propose that the decreased resistance to IR in DAB2IP-expressing C4-2 cells may be partially due to the inhibition of autophagy.

DAB2IP Inhibits Autophagy through the mTOR-S6K Pathway

To further explore the role of DAB2IP in autophagy, we determined the expression levels of the microtubule-associated protein LC3B. LC3B exists in a cytosolic form, LC3B-I, and an LC3B-II form that is conjugated to phosphatidylethanolamine [16,17]. Increased LC3B-II levels are closely associated with the number of autophagosomes and serve as a good indicator of autophagosome formation [18]. As shown in Figure 5, *A* and *B*, increased DAB2IP impairs both IR- and NU7441-mediated induction of LC3B-II in C4-2 cells. In addition, the lower expression of Beclin 1 protein was noticed in DAB2IP-expressing C4-2 cells.

It is reported that Akt-mTOR pathway negatively regulates autophagy [19]. To investigate how this signaling cascade is operated in DAB2IP-associated autophagy inhibition in C4-2 cells, we measured phosphorylation of mTOR in both cell lines (Figure 5). Compared

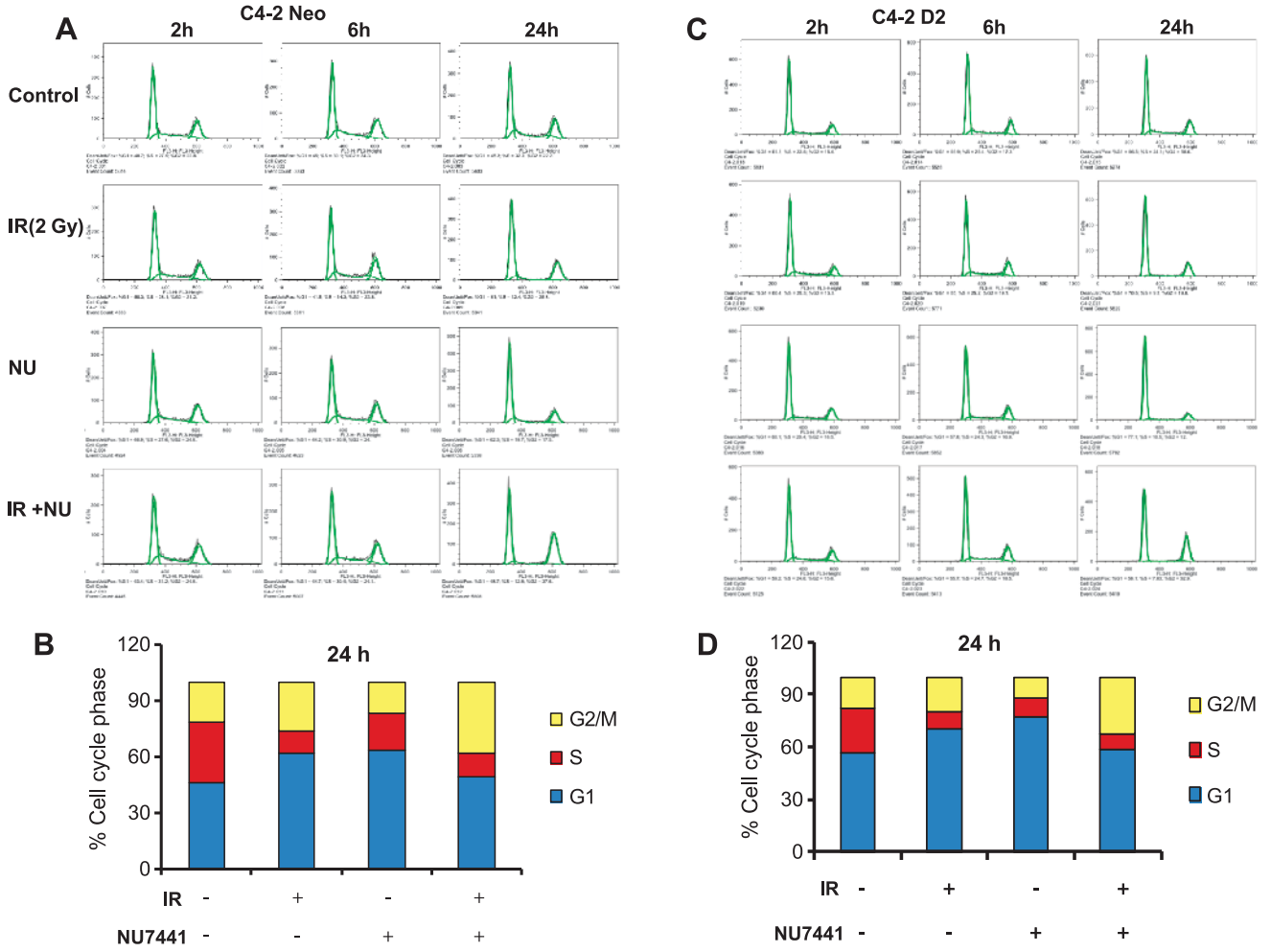

Figure 3. Cell cycle analysis in DAB2IP-negative and DAB2IP-positive PCa cells after treatment with NU7441 and IR. C4-2 D2 and C4-2 neo cells were treated with IR (2 Gy), NU7441 (2 μM), and IR + NU7441 as indicated. Samples were collected at 0, 2, 6, and 24 hours post-treatment. Propidium iodide (PI) staining was used to detect the distribution of cells after various treatments. (A and B) C4-2 neo cells and (C and D) C4-2D2 cells.

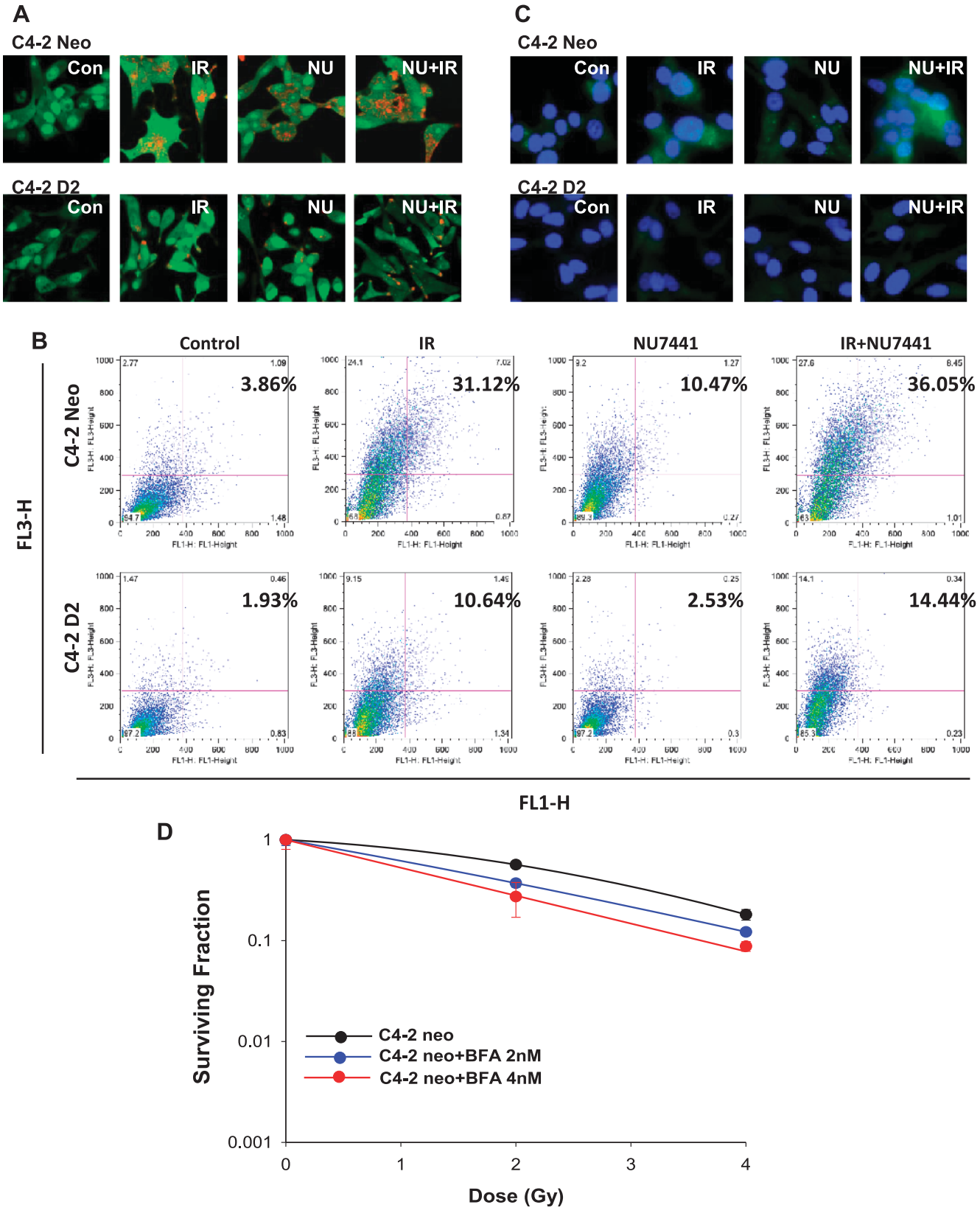

Figure 4. DAB2IP expression suppressed IR- or NU7441 + IR–induced autophagy in PCa cells. C4-2 neo and D2 cells were treated with NU744, IR, and IR + NU7441 for 72 hours and then stained with AO. (A) Fluorescent images of AVO-positive cells. (B) Flow cytometry analysis to assess autophagy and (C) immunofluorescence staining of LC3B antibody. Experiments in A to C were performed under identical conditions. (D) SF analysis of C4-2 neo cells after combined treatment of IR and an autophagy inhibitor Baf A1 as indicated.

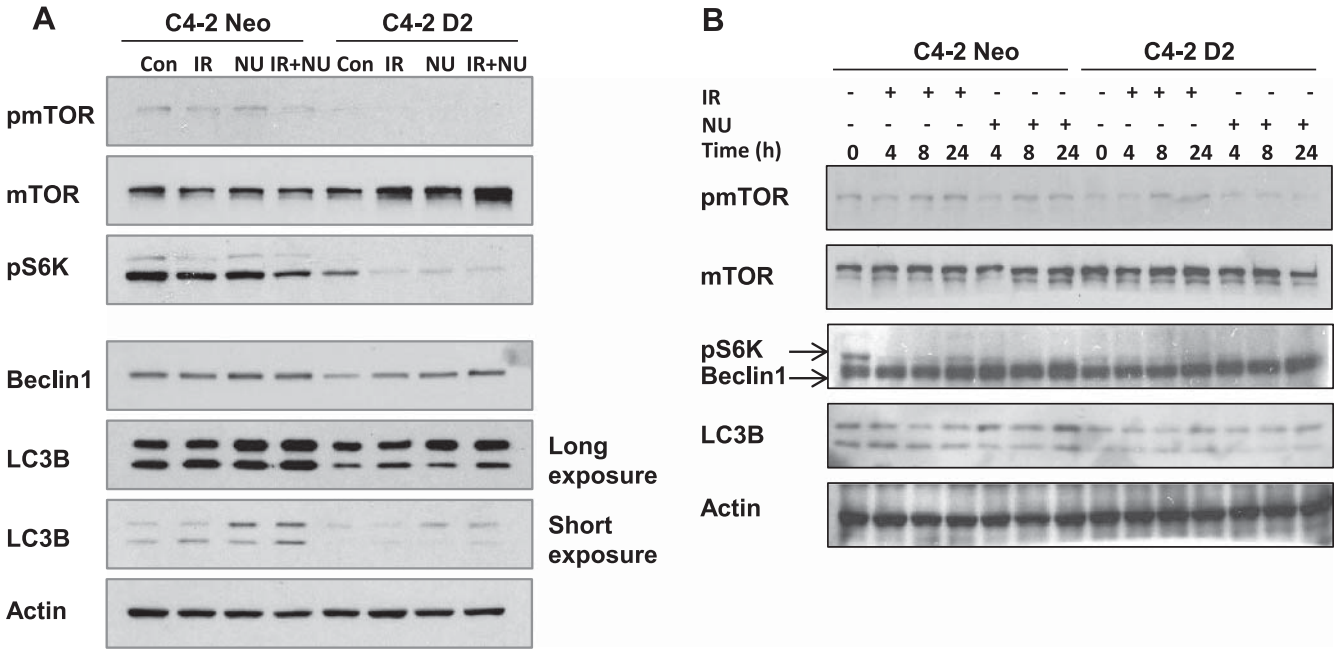

Figure 5. DAB2IP inactivates mTOR-S6K pathway and suppresses the expression of autophagy-associated proteins. (A) The phosphorylation of mTOR and S6K and the expression of autophagy-associated Beclin 1 and LC3B were determined by Western blot analysis 24 hours after IR (5 Gy). (B) The phosphorylation of mTOR and S6K and the expression of autophagy-associated Beclin 1 and LC3B were determined by Western blot analysis at the indicated time points.

with C4-2 neo cells, there was a dramatic inhibition of phosphorylated mTOR in C4-2 D2 cells. Furthermore, studies have shown that S6K is a critical downstream effector of the mTOR signaling pathway [20]. We observed decreased phosphorylation of S6K in DAB2IP-overexpressed C4-2 D2 cells (Figure 5). Although mTOR-S6K activation is known to suppress autophagy in mammalian cells, emerging studies have indicated that, in certain situations, the mTOR-S6K pathway positively regulates autophagy [21–23]. Together, our findings show that DAB2IP may suppress IR- and NU7441-induced autophagy through the mTOR-S6K pathway.

DAB2IP Promotes Apoptosis in Response to Combined Treatment of NU7441 and IR

It is reported that autophagy is an adaptive mechanism that can cause resistance to therapy-induced apoptosis [24]. In previous experiments, we noticed that DAB2IP acts as an autophagy inhibitor and can promote apoptosis in response to therapeutic agents. To explore, we examine IR- and NU7441-induced apoptosis in C4-2 cells with or without DAB2IP. Cells were fixed and stained with DAPI 12 hours after NU7441 or/and IR treatment. As shown in Figure 6*A*, little or no significant apoptotic event was noticed after IR or NU7441 treatment alone, in either DAB2IP-negative or DAB2IP-positive cells. However, C4-2D2 cells showed enhanced apoptosis (7.8%) after combined treatment of IR + NU7441 after 12 hours, whereas C4-2 neo cells showed only 3.8% at the same time (Figure 6*B*; $P < .05$). For further characterization, Western blot analysis was performed to analyze cleaved PARP-1 (Figure 6*C*). We noticed that the PARP-1 cleavage is greater (lane 8) in C4-2D2 cells when compared to neo cells (lane 4) in response to IR + NU7441. These results suggest that DAB2IP can promote cell death in PCa cells by blocking autophagy when treated with IR + NU7441.

Loss of DAB2IP Correlates with Decreased BRFS

To determine whether loss of DAB2IP in PCa results in clinically relevant radiation resistance, we performed a retrospective cohort study of high-risk (PCa) patients treated with definitive RT (Figure 7). Patient's DAB2IP status was determined using IHC and patients were followed for biochemical recurrence as mentioned in Materials and Methods section. Twenty-four patients treated for high-risk PCa were evaluated. DAB2IP loss was seen in 8 patients (33.3%), whereas 16 patients (66.7%) expressed DAB2IP. Median follow-up for DAB2IP patients was 19.4 months (range, 8.2 to 57.8 months) and 23.9 months (range, 8.8 to 74.0 months) for the DAB2IP-deficient group. Patients expressing DAB2IP exhibited markedly improved BRFS compared to patients with loss of DAB2IP ($P = .027$; log-rank test). The estimated 2-year BRFS was 90% and 68.5%, respectively, for the DAB2IP-present and DAB2IP-deficient groups. At 4 years, BRFS was 90% and 34.3% for the present and deficient groups, respectively. Univariate analysis demonstrated DAB2IP status as the only variable with significant association to BRFS at this point of follow-up.

Discussion

DAB2IP/AIP1, a potential tumor suppressor gene, is often down-regulated in PCa primarily due to altered epigenetic regulation of its promoter [25]. It functions as a key scaffold protein to modulate cell proliferation, survival, and apoptosis by coordinating PI3K, Akt, and the ASK1 pathway [26,27]. Our previous work indicated that loss of DAB2IP expression in PCa cells greatly increases radiation resistance *in vitro* [5,6]. To determine whether our previous *in vitro* findings were clinically relevant, we performed a retrospective cohort study and determined that loss of DAB2IP leads to significantly increased rates of biochemical failure after RT (Figure 7).

DNA-PKcs, a key component of the NHEJ pathway, plays a dominant role in DNA DSB repair, genomic integrity, and maintaining telomere stability [7,28] and is upregulated in various cancers [29,30]. It is also reported that increased DNA-PKcs expression and kinase activity are closely associated with radioresistance or chemoresistance [31,32]. Inhibitors of DNA-PKcs such as NU7441 have been developed to enhance RT-based local tumor control [33]. In this study, we clearly show that adjuvant treatment with NU7441 can overcome PCa radioresistance caused by loss of DAB2IP (Figure 1). NU7441-mediated radiosensitization in PCa cells is mainly contributed to delayed IR-induced DSB repair. A recent study in glioma-initiating cells demonstrated that DNA-PKcs is involved in autophagy in response to irradiation. In these cells, suppression of DNA-PKcs sensitizes cells to IR-induced autophagic cell death [11].

NU7441 is also known to inhibit PI3K-Akt [33], which is the upstream of mTOR signaling pathway. Therefore, we have used the inhibitors of PI3K (LY294002) and mTOR (rapamycin and RAD001) pathways to test the radiosensitivity in DAB2IP-deficient PCa (C4-2 neo) cells. In addition, we used a dual kinase inhibitor NVP-BEZ235 that blocks both PI3K and mTOR signaling. Our results showed that all three inhibitors exhibit radiation sensitivity of C4-2 neo cells. The maximum radiosensitivity was achieved using NVP-BEZ235, which indicates that both PI3K and mTOR pathways were involved in the increased radioresistance of C4-2 neo cells (Figure W1, *A* and *B*). Furthermore, we used LY294002, an inhibitor of the PI3K pathway in combination with radiation, which showed a strong radiosensitizing effect in C4-2 neo cells (Figure W1*A*). We have performed Western blot analyses to confirm that these inhibitors blocked the PI3K (inhibition of pAKT) and mTOR (inhibition of pS6K) signaling pathways (Figure W1, *C* and *D*).

Autophagy is a lysosomal degradation pathway that eliminates damage or potentially dangerous proteins and organelles under adverse conditions to protect organisms from metabolic stress [34]. Many studies have shown that cancer cells use autophagy as an adaptive and context-dependent system to overcome radiotherapeutic stress, autophagy increases in tumor cells in response to radiation and DNA damage, and radioresistance may be associated with autophagy induction [15,35–37]. On the basis of these evidences, autophagy-related pathway has been considered as a potential and important therapeutic target in radiation oncology. Therefore, we performed experiments to determine whether the inhibition of DNA-PKcs can induce autophagy in DAB2IP-deficient PCa cells and the precise role of this catabolic process in radiation resistance. In this study, AVO staining was used to compare cellular autophagy response to IR with or without NU7441 treatment. We noticed that NU7441 treatment can promote both IR-induced and basal level of cell autophagy. The autophagy marker protein LC3B is induced upon treatment with NU7441 (Figure 4).

In addition to DNA-PKcs, our expected results showed that DAB2IP is also involved in autophagy pathway and overexpression of this gene attenuated IR- and NU7441-induced autophagy. Furthermore, we

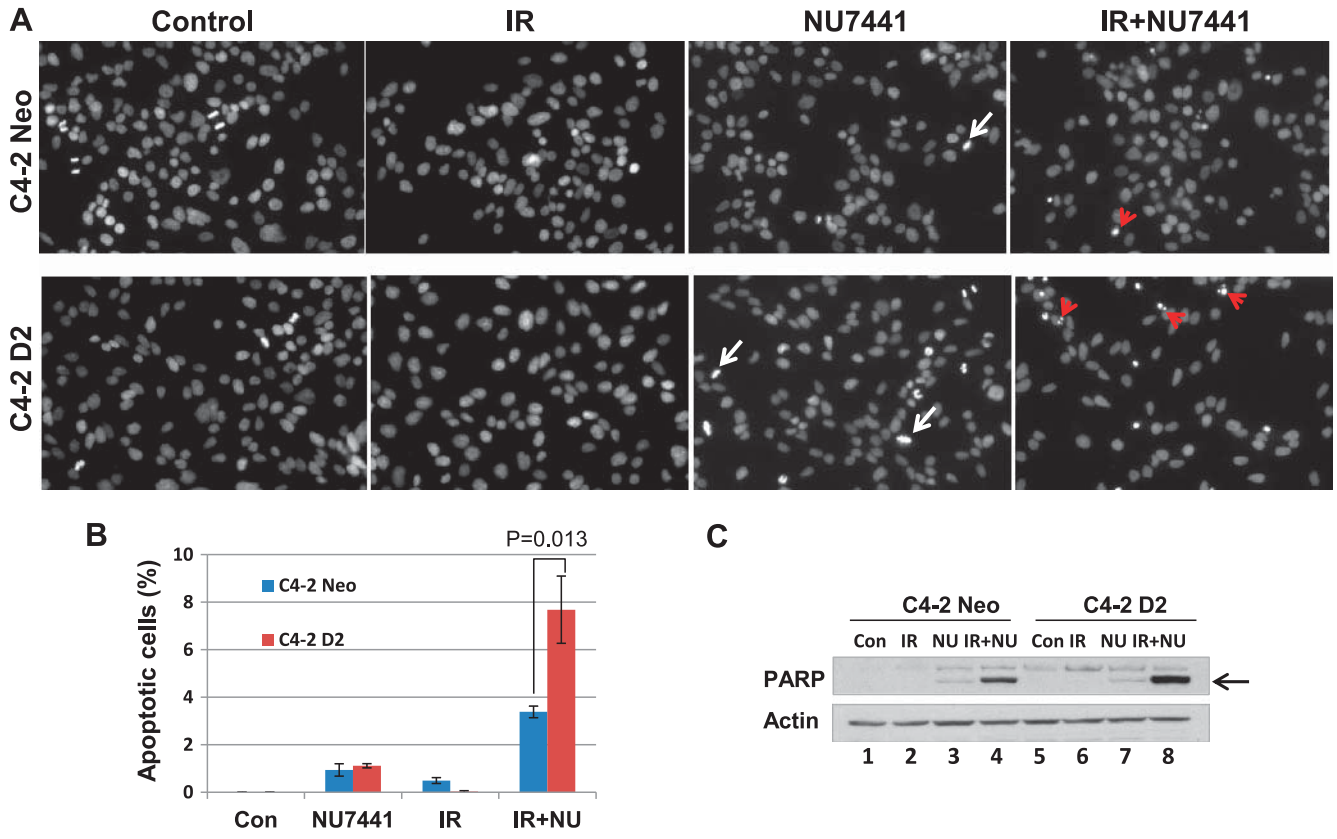

Figure 6. DAB2IP promotes apoptosis in response to IR + NU7441. (A) IR + NU7441–induced apoptosis was determined by DAPI staining. Cells were treated with +/− NU7441 and IR (10 Gy) for 12 hours and the cells were stained with DAPI; the representative fluorescence images are shown. White arrows indicated the mitotic cells and the red arrows represent the apoptotic cells. (B) Quantitative analysis of apoptotic cells. The data are presented as the means ± SD of three independent experiments. (C) Analysis of PARP cleavage. Cells were lysed 12 hours after exposure to IR or IR + NU7441 and subjected to Western blot analysis.

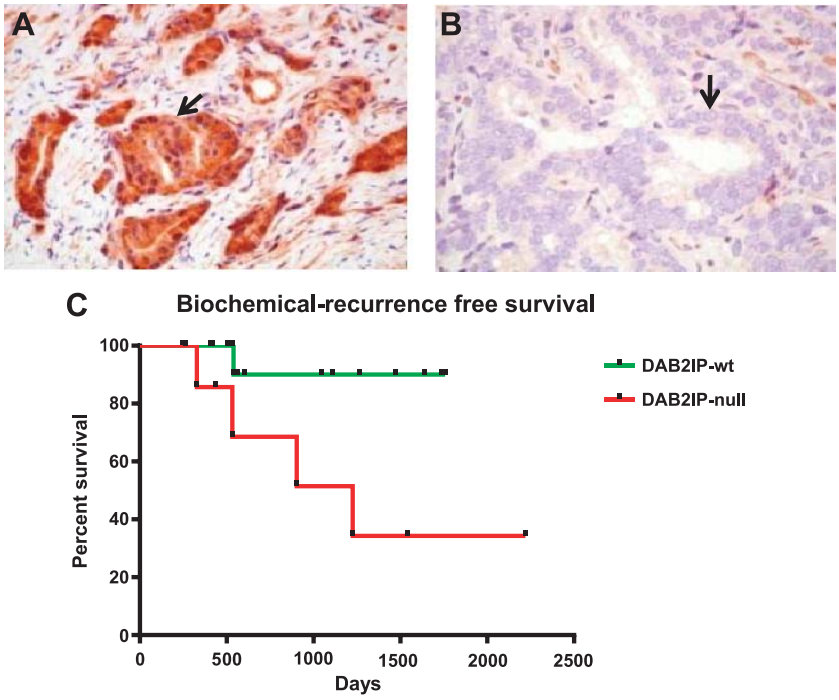

Figure 7. IHC staining of DAB2IP in high-risk PCa patients. (A) Representative patients with positive DAB2IP expression. (B) Representative patient with DAB2IP loss. (C) BRFS plotted by patients' DAB2IP status.

observed that LC3B and Beclin 1 are downregulated in cells expressing DAB2IP. These results suggest that DAB2IP mediated radiosensitization of PCa cells partially through inhibition of autophagy. To further prove this, we treated PCa cells with autophagy inhibitor Baf A1 after irradiation. We found that Baf A1 significantly enhanced radiation sensitivity (Figure 4*D*). The mTOR-S6K pathway is postulated to be a negative regulator of mammalian autophagy [19]. In contrast, we show that mTOR-S6K pathway was inactivated in DAB2IP-expressing PCa cells. Studies show that mTOR can also positively modulate autophagy. Klionsky et al. reported that mTOR inhibition by rapamycin or siRNA-mediated silencing of S6K expression reduced 6-thioguanine–induced autophagy in human colorectal cancer cells [23]. Scott et al. suggested that S6K is essential for autophagy in fat cells of *Drosophila* [22]. Consistent with these reports, our results showed that phosphorylation of S6K was almost totally attenuated in DAB2IP-expressing PCa cells. Notably, DAB2IP functions as a scaffold protein to inhibit the PI3K-Akt pathway using a direct protein interaction with PI3K through its PR domain [26].

Autophagy-defective cells also show an increase in DNA-DSB in response to various stresses, including IR [13,38]. To further evaluate the role of autophagy in DNA-DSB repair, we found that DAB2IP-proficient PCa cells exhibit higher level of DNA damage compared to control cells after IR treatment. We believe that the inhibition of autophagy in DAB2IP-proficient cells is the major contributing factor toward the impaired DNA damage. Moreover, recent work indicates that autophagy can promote tumor cell survival and inhibition of autophagy leads to significant tumor regression [39]. It is conceivable that DAB2IP inhibits autophagy that could contribute to the suppression of tumor growth and aggressiveness.

In summary, the results of this study demonstrate that inhibition of DNA-PKcs enhances the effect of IR in DAB2IP-deficient radioresistant human PCa cells. Moreover, our findings demonstrate a role for DAB2IP in inhibiting mTOR-S6K pathway and suppressing autophagy. On the basis of these results, DAB2IP appears to be an excellent RT target in the treatment of PCa.

References

[1] Jemal A, Siegel R, Ward E, Hao Y, Xu J, and Thun MJ (2009). Cancer statistics, 2009. *CA Cancer J Clin* **59**, 225–249.

[2] Hanks GE, Pajak TF, Porter A, Grignon D, Brereton H, Venkatesan V, Horwitz EM, Lawton C, Rosenthal SA, Sandler HM, et al. (2003). Phase III trial of long-term adjuvant androgen deprivation after neoadjuvant hormonal cytoreduction and radiotherapy in locally advanced carcinoma of the prostate: the Radiation Therapy Oncology Group Protocol 92-02. *J Clin Oncol* **21**, 3972–3978.

[3] Tomioka A, Tanaka M, De Velasco MA, Anai S, Takada S, Kushibiki T, Tabata Y, Rosser CJ, Uemura H, and Hirao Y (2008). Delivery of PTEN via a novel gene microcapsule sensitizes prostate cancer cells to irradiation. *Mol Cancer Ther* **7**, 1864–1870.

[4] Chen H, Pong RC, Wang Z, and Hsieh JT (2002). Differential regulation of the human gene DAB2IP in normal and malignant prostatic epithelia: cloning and characterization. *Genomics* **79**, 573–581.

[5] Kong Z, Xie D, Boike T, Raghavan P, Burma S, Chen DJ, Habib AA, Chakraborty A, Hsieh JT, and Saha D (2010). Downregulation of human DAB2IP gene expression in prostate cancer cells results in resistance to ionizing radiation. *Cancer Res* **70**, 2829–2839.

[6] Kong Z, Raghavan P, Xie D, Boike T, Burma S, Chen D, Chakraborty A, Hsieh JT, and Saha D (2010). Epothilone B confers radiation dose enhancement in DAB2IP gene knock-down radioresistant prostate cancer cells. *Int J Radiat Oncol Biol Phys* **78**, 1210–1218.

[7] Lee SH and Kim CH (2002). DNA-dependent protein kinase complex: a multifunctional protein in DNA repair and damage checkpoint. *Mol Cells* **13**, 159–166.

[8] Woo RA, Jack MT, Xu Y, Burma S, Chen DJ, and Lee PW (2002). DNA damage-induced apoptosis requires the DNA-dependent protein kinase, and is mediated by the latent population of p53. *EMBO J* **21**, 3000–3008.

[9] Callen E, Jankovic M, Wong N, Zha S, Chen HT, Difilippantonio S, Di Virgilio M, Heidkamp G, Alt FW, Nussenzweig A, et al. (2009). Essential role for DNA-PKcs in DNA double-strand break repair and apoptosis in ATM-deficient lymphocytes. *Mol Cell* **34**, 285–297.

[10] Shaheen FS, Znojek P, Fisher A, Webster M, Plummer R, Gaughan L, Smith GC, Leung HY, Curtin NJ, and Robson CN (2011). Targeting the DNA double strand break repair machinery in prostate cancer. *PloS One* **6**, e20311.

[11] Daido S, Yamamoto A, Fujiwara K, Sawaya R, Kondo S, and Kondo Y (2005). Inhibition of the DNA-dependent protein kinase catalytic subunit radiosensitizes malignant glioma cells by inducing autophagy. *Cancer Res* **65**, 4368–4375.

[12] Yang ZJ, Chee CE, Huang S, and Sinicrope FA (2011). The role of autophagy in cancer: therapeutic implications. *Mol Cancer Ther* **10**, 1533–1541.

[13] Bae H and Guan JL (2011). Suppression of autophagy by FIP200 deletion impairs DNA damage repair and increases cell death upon treatments with anticancer agents. *Mol Cancer Res* **9**, 1232–1241.

[14] Edinger AL and Thompson CB (2003). Defective autophagy leads to cancer. *Cancer Cell* **4**, 422–424.

[15] Apel A, Herr I, Schwarz H, Rodemann HP, and Mayer A (2008). Blocked autophagy sensitizes resistant carcinoma cells to radiation therapy. *Cancer Res* **68**, 1485–1494.

[16] Tanida I, Ueno T, and Kominami E (2004). LC3 conjugation system in mammalian autophagy. *Int J Biochem Cell Biol* **36**, 2503–2518.

[17] Sou YS, Tanida I, Komatsu M, Ueno T, and Kominami E (2006). Phosphatidylserine in addition to phosphatidylethanolamine is an *in vitro* target of the mammalian Atg8 modifiers, LC3, GABARAP, and GATE-16. *J Biol Chem* **281**, 3017–3024.

[18] Rouschop KM, van den Beucken T, Dubois L, Niessen H, Bussink J, Savelkouls K, Keulers T, Mujcic H, Landuyt W, Voncken JW, et al. (2010). The unfolded protein response protects human tumor cells during hypoxia through regulation of the autophagy genes MAP1LC3B and ATG5. *J Clin Invest* **120**, 127–141.

[19] Kondo Y, Kanzawa T, Sawaya R, and Kondo S (2005). The role of autophagy in cancer development and response to therapy. *Nat Rev Cancer* **5**, 726–734.

[20] Zoncu R, Efeyan A, and Sabatini DM (2011). mTOR: from growth signal integration to cancer, diabetes and ageing. *Nat Rev Mol Cell Biol* **12**, 21–35.

[21] Zeng X and Kinsella TJ (2008). Mammalian target of rapamycin and S6 kinase 1 positively regulate 6-thioguanine-induced autophagy. *Cancer Res* **68**, 2384–2390.

[22] Scott RC, Schuldiner O, and Neufeld TP (2004). Role and regulation of starvation-induced autophagy in the *Drosophila* fat body. *Dev Cell* **7**, 167–178.

[23] Klionsky DJ, Meijer AJ, and Codogno P (2005). Autophagy and p70S6 kinase. *Autophagy* **1**, 59–60; discussion 60–51.

[24] Amaravadi RK, Yu D, Lum JJ, Bui T, Christophorou MA, Evan GI, Thomas-Tikhonenko A, and Thompson CB (2007). Autophagy inhibition enhances therapy-induced apoptosis in a Myc-induced model of lymphoma. *J Clin Invest* **117**, 326–336.

[25] Chen H, Tu SW, and Hsieh JT (2005). Down-regulation of human DAB2IP gene expression mediated by polycomb Ezh2 complex and histone deacetylase in prostate cancer. *J Biol Chem* **280**, 22437–22444.

[26] Xie D, Gore C, Zhou J, Pong RC, Zhang H, Yu L, Vessella RL, Min W, and Hsieh JT (2009). DAB2IP coordinates both PI3K-Akt and ASK1 pathways for cell survival and apoptosis. *Proc Natl Acad Sci USA* **106**, 19878–19883.

[27] Xie D, Gore C, Liu J, Pong RC, Mason R, Hao G, Long M, Kabbani W, Yu L, Zhang H, et al. (2010). Role of DAB2IP in modulating epithelial-to-mesenchymal transition and prostate cancer metastasis. *Proc Natl Acad Sci USA* **107**, 2485–2490.

[28] Hefferin ML and Tomkinson AE (2005). Mechanism of DNA double-strand break repair by non-homologous end joining. *DNA Repair (Amst)* **4**, 639–648.

[29] Um JH, Kwon JK, Kang CD, Kim MJ, Ju DS, Bae JH, Kim DW, Chung BS, and Kim SH (2004). Relationship between antiapoptotic molecules and metastatic potency and the involvement of DNA-dependent protein kinase in the chemosensitization of metastatic human cancer cells by epidermal growth factor receptor blockade. *J Pharmacol Exp Ther* **311**, 1062–1070.

[30] Tonotsuka N, Hosoi Y, Miyazaki S, Miyata G, Sugawara K, Mori T, Ouchi N, Satomi S, Matsumoto Y, Nakagawa K, et al. (2006). Heterogeneous expression of DNA-dependent protein kinase in esophageal cancer and normal epithelium. *Int J Mol Med* **18**, 441–447.

[31] Shintani S, Mihara M, Li C, Nakahara Y, Hino S, Nakashiro K, and Hamakawa H (2003). Up-regulation of DNA-dependent protein kinase correlates with radiation resistance in oral squamous cell carcinoma. *Cancer Sci* **94**, 894–900.

[32] Beskow C, Skikuniene J, Holgersson A, Nilsson B, Lewensohn R, Kanter L, and Viktorsson K (2009). Radioresistant cervical cancer shows upregulation of the NHEJ proteins DNA-PKcs, Ku70 and Ku86. *Br J Cancer* **101**, 816–821.

[33] Leahy JJ, Golding BT, Griffin RJ, Hardcastle IR, Richardson C, Rigoreau L, and Smith GC (2004). Identification of a highly potent and selective DNA-dependent protein kinase (DNA-PK) inhibitor (NU7441) by screening of chromenone libraries. *Bioorg Med Chem Lett* **14**, 6083–6087.

[34] Kroemer G, Marino G, and Levine B (2010). Autophagy and the integrated stress response. *Mol Cell* **40**, 280–293.

[35] Alva AS, Gultekin SH, and Baehrecke EH (2004). Autophagy in human tumors: cell survival or death? *Cell Death Differ* **11**, 1046–1048.

[36] Bergmann A (2007). Autophagy and cell death: no longer at odds. *Cell* **131**, 1032–1034.

[37] Chaachouay H, Ohneseit P, Toulany M, Kehlbach R, Multhoff G, and Rodemann HP (2011). Autophagy contributes to resistance of tumor cells to ionizing radiation. *Radiother Oncol* **99**, 287–292.

[38] Mathew R, Kongara S, Beaudoin B, Karp CM, Bray K, Degenhardt K, Chen G, Jin S, and White E (2007). Autophagy suppresses tumor progression by limiting chromosomal instability. *Genes Dev* **21**, 1367–1381.

[39] Kimmelman AC (2011). The dynamic nature of autophagy in cancer. *Genes Dev* **25**, 1999–2010.

Supplementary Methods

Clonogenic Survival Assay

Exponentially growing cells were trypsinized and counted using a Coulter counter (Beckman Coulter). Cells were diluted serially to appropriate concentrations and plated onto 60-mm dishes in triplicates. After 3 hours of incubation, cells were treated with increasing doses of IR (2, 4, 6, and 8 Gy) or indicated drugs (25 nM NVP-BEZ235, 10 μM LY294002, 100 nM rapamycin, or 10 nM RAD001) or drugs + IR. For NVP-BEZ235 treatment, drug-containing medium was replaced with drug-free medium at 16 hours after IR. After 10 to 14 days, cells were fixed and stained with 4% formaldehyde and 0.05% crystal violet in PBS. Colonies containing >50 cells were counted. SF was calculated as (mean colony counts)/[(cells inoculated) × (plating efficiency)], in which plating efficiency was defined as (mean colony counts)/(cells inoculated for unirradiated controls). The data are presented as means ± SD of at least three independent experiments. The curve $S = e^{-(\alpha D + \beta D2)}$ was fitted to the experimental data using a least-squares fit algorithm using the program Sigma Plot 11.0 (Systat Software, Inc).

Western Blot Analysis

C4-2 neo cells were treated with LY294002 (10 μM), NVP-BEZ235 (25 nM), rapamycin (100 nM), and RAD001 (10 nM) as indicated for 1 hour, followed by radiation (10 Gy). After 1 hour, cells were lysed and Western blot analysis was performed.

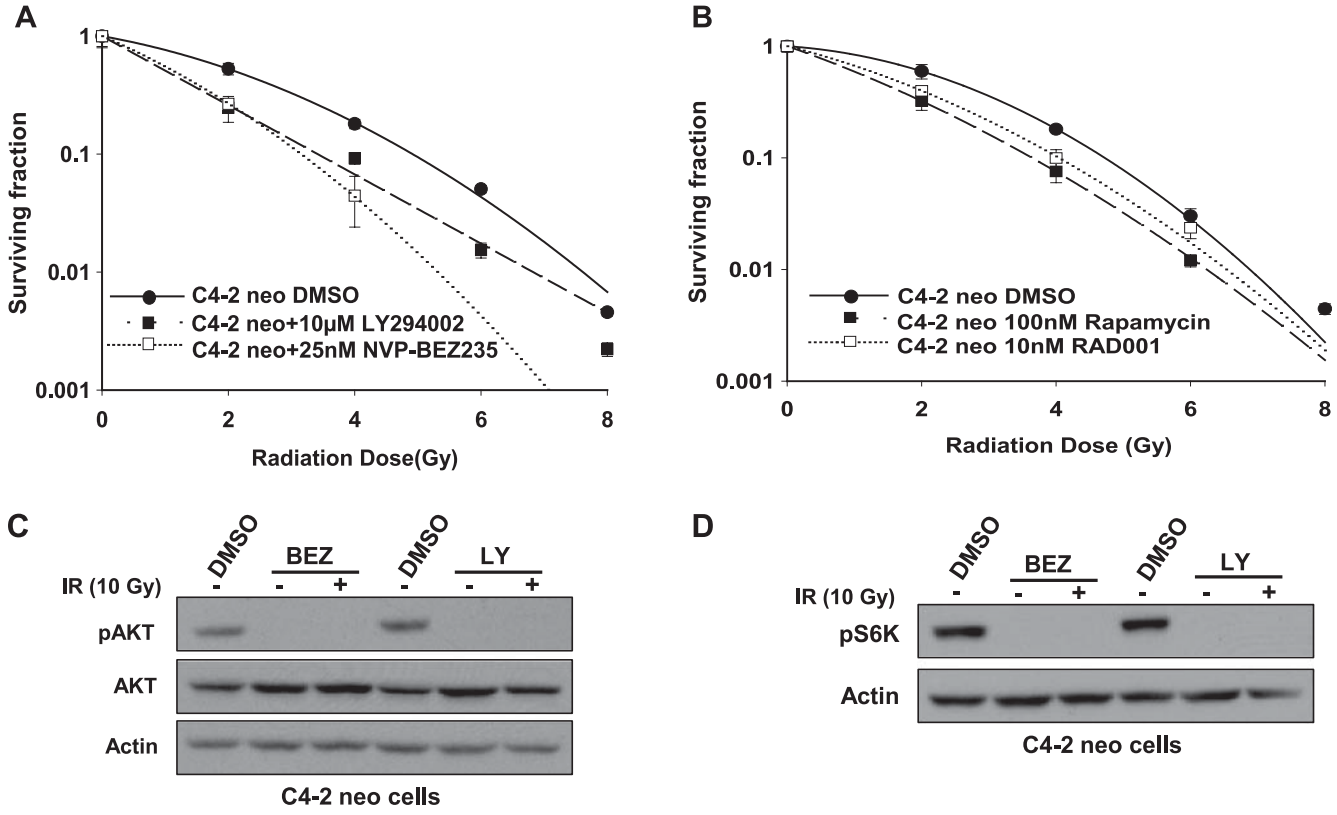

Figure W1. PI3K-AKT and PI3K-mTOR inhibitors increase the radiosensitivity in DAB2IP-negative PCa cell line. (A) The SF analysis of C4-2 neo cells after combined treatment with 10 μM LY294002 and IR or 25 nM NVP-BEZ235 and IR. (B) SF analysis of C4-2 neo cells after combined treatment with 100 nM rapamycin and IR or 10 nM RAD001. (C) C4-2 neo cells were irradiated (10 Gy) after 1 hour of 10 μM LY294002 or 25 nM NVP-BEZ235 treatment and harvested at 1 hour after IR. Inhibition of PI3K-Akt pathway was analyzed by Western blot analysis with phospho-Akt (Ser^{473}) antibody. (D) C4-2 neo cells were irradiated (10 Gy) after 1 hour of 100 nM rapamycin or 10 nM RAD001 treatment and harvested at 1 hour after IR. Inhibition of mTOR pathway was analyzed by Western blot analysis with phospho-S6K antibody.

Development of a locally advanced orthotopic prostate tumor model in rats for assessment of combined modality therapy

VASU TUMATI[1], SANJEEV MATHUR[6], KWANG SONG[1], JER-TSONG HSIEH[2,7], DAWEN ZHAO[3,7], MASAYA TAKAHASHI[4], TIMOTHY DOBIN[2], LEAH GANDEE[2], TIMOTHY D. SOLBERG[1,7], AMYN A. HABIB[5,7] and DEBABRATA SAHA[1,7]

Departments of [1]Radiation Oncology, [2]Urology, [3]Radiology, [4]Advanced Imaging, [5]Neurology, University of Texas Southwestern Medical Center, Dallas, TX 75390; [6]Uniformed Services University of Health Sciences (USUHS), Bethesda, MD 20814; [7]Simmons Comprehensive Cancer Center, Dallas, TX 75390, USA

Received December 26, 2012; Accepted February 13, 2013

DOI: 10.3892/ijo.2013.1858

Abstract. The purpose of this study was to develop an aggressive locally advanced orthotopic prostate cancer model for assessing high-dose image-guided radiation therapy combined with biological agents. For this study, we used a modified human prostate cancer (PCa) cell line, PC3, in which we knocked down a tumor suppressor protein, DAB2IP (PC3-KD). These prostate cancer cells were implanted into the prostate of nude or Copenhagen rats using either open surgical implantation or a minimally invasive procedure under ultrasound guidance. We report that: i) these DAB2IP-deficient PCa cells form a single focus of locally advanced aggressive tumors in both nude and Copenhagen rats; ii) the resulting tumors are highly aggressive and are poorly controlled after treatment with radiation alone; iii) ultrasound-guided tumor cell implantation can be used successfully for tumor development in the rat prostate; iv) precise measurement of the tumor volume and the treatment planning for radiation therapy can be obtained from ultrasound and MRI, respectively; and v) the use of a fiducial marker for enhanced radiotherapy localization in the rat orthotopic tumor. This model recapitulates radiation-resistant prostate cancers which can be used to demonstrate and quantify therapeutic response to combined modality treatments.

Introduction

Prostate cancer is one of the most common male cancers, representing 28% of all male cancers in 2010 (1). In addition, prostate cancer was the second most common cause of cancer related death in US men (1). Treatment of prostate cancer can range from careful monitoring to treatment with prostatectomy or radiation. In most cases radical radiation therapy is very effective with 5 year local control rates of up to 89% (2). However, a proportion of patients will fail initial therapy and present with recurrent advanced local and distant metastatic disease. No curative treatment currently exists for those patients who present with recurrent disease.

In recent years, there has been a rise in the use of image guided radiation therapy (IGRT) in the treatment of prostate cancer. Because the prostate is a mobile organ, inter and intra fraction movement, as well as random deformation of the organ, can occur throughout the course of daily radiation treatment (3). Crevoisier *et al* showed that failure to compensate for daily prostate motion may lead to poorer clinical outcomes (4). Prostate position can be monitored through the use of fiducial markers that are visible on radiographic images. By using daily imaging it is possible to achieve accurate prostate localization and ensure homogeneous dose distributions.

While the use of image-guidance has improved the accuracy of radiotherapy, allowing safe and effective dose escalation in the treatment of primary prostate cancer, there is still no effective therapy for aggressive or recurrent disease. To develop effective therapies for aggressive prostate cancer, whether novel or a combination of several agents and treatment modalities, it is imperative to first develop a model of radiation resistant prostate cancer.

To facilitate the investigation of resistant aggressive disease after radiation in a preclinical environment it would be best to have a locally advanced orthotopic rodent model. In this study we report the development of such a model for resistant tumors after IGRT in rat prostates using a novel tumor suppressor knockdown prostate cancer cell line.

Materials and methods

Cell culture. Human PCa cell line PC3 was modified by knocking down the tumor suppressor protein DAB2IP (PC3-KD) and co-transfected with luciferase reporter gene as described

Correspondence to: Dr Debabrata Saha, Department of Radiation Oncology, University of Texas Southwestern Medical Center, 2201 Inwood Road, Dallas, TX 75390-9187, USA
E-mail: debabrata.saha@utsouthwestern.edu

Key words: prostate cancer, radioresistance, animal MRI, ultrasound and image-guided radiation therapy

previously by Kong *et al* (5). Cells were cultured in T medium supplemented with 5% fetal calf serum, 100 U/ml penicillin, 100 μg/ml streptomycin, 900 μg/ml of G418, and 700 ng/ml of puromycin in an atmosphere of 95% air/5% CO_2 at 37°C.

Orthotopic model. A total of $1x10^5$ PC3-KD cells were diluted to a final volume of 30 μl. Male rats, either nude or Copenhagen, were anesthetized using 1-2% isoflurane mixed with 100% O_2. Cells were injected into the right lobe of prostate and a gold fiducial marker was placed into the prostate for subsequent image guided therapy. All the experiments were conducted under UT Southwestern Institutional Animal Care and Use Committee-approved guidelines for animal welfare.

Ultrasound. Ultrasound imaging was employed for i) minimally invasive implantation of tumor cells; ii) measuring tumor volume in the rat prostate. For implantation, rats were anesthetized and the pelvis was shaved and sterilized. Animals were secured to the handling table to ensure no movement. The prostate and bladder was identified in the field of view by using an RMV716 transducer head (VisualSonics Vevo® 770 Imaging System, Amsterdam, The Netherlands). Once the prostate was visualized, a gold seed was implanted into the prostate using an 18G needle mounted on a trocar. The needle was aligned parallel to the transducer and inserted parallel to the urethra. After confirming proper placement of the fiducial, the needle was left in place and cells were implanted using a 1cc syringe. Imaging was performed on the VisualSonics Vevo 770 Imaging System using the real-time Micro Visualization scan head RMV716 (11-24 MHz) specific for rats. Rats were anesthetized and the transducer head was placed transverse to the pelvis of the rats in supine position. Images were obtained by resolving various depths of tissue into the center of optimum resolution plane to ensure clear images throughout the tumor volume.

Bioluminescence imaging. BL imaging was performed weekly using an IVIS Lumina Imaging System (Xenogen, Alameda, CA). Rats were anesthetized by using isoflurane inhalation mixed in pure oxygen followed by an i.p. injection of D-luciferin (80 mg/kg). BL images were acquired 10 min after luciferin injection using various exposure times.

Colony formation assay. Surviving fraction (SF) analysis was performed using PC3 Con (DAB2IP proficient) and PC3-KD (DAB2IP deficient) as described by Kong *et al* (5,6). In brief, cells were counted, serially diluted and plated in 60 mm dishes. After 6 h, treated with increasing doses of radiation (0 to 8 Gy) and then incubated 10 days for colony formation. Colonies were counted and SF curves were plotted using linear quadratic equation (Sigma plot 11.0, Systat Software, Inc).

Magnetic resonance imaging. MRI studies were conducted using a 3 Tesla whole-body human scanner (Achieva™, Philips Medical Systems, Best, The Netherlands) with a small animal solenoid radio-frequency (RF) coil (63 mm in diameter and 100 mm in length; Philips Research Europe, Hamburg, Germany). Under anesthesia, animals were placed supine where the thigh of the rat centered with respect to the center of the RF coil. A volume containing the entire tumor was subsequently obtained using T2 weighted multi-slice fast spin echo sequences (repetition time, 5,700 msec; echo time, 70 msec; slice thickness, 2 mm; field of view, 75 x 48 x 50 mm in-plain resolution of 0.26 x 0.29 mm) and three dimensional gradient sequences (repetition time, 7.7 msec; echo time, 4.5 msec; flip angle 15, field of view = 75 x 51 x 50 mm resolution of 0.7 mm^3 isotropic voxel).

Microirradiation. Radiation was carried out using an X-ray image guided small animal irradiator as previously described (7,8). The irradiator is characterized by a high dose rate, small beam size, accurate and precise target localization facilitated through image guidance, resulting in precision-high dose irradiation. The collimation system consists of a 2.5-cm-thick brass alloy disk with interchangeable apertures ranging from 1 to 20 mm in nominal diameter.

H&E staining. Prostate tumors were removed and fixed in 4% formalin. Tumors were mounted in paraffin and sections (10 μm) were prepared for standard H&E staining. Briefly, sections were deparaffinized, rehydrated, stained with Harris's hematoxylin for 20 sec followed by treatment with Scott's solution. After washings, sections were stained with eosin for 2 min, rinsed, dehydrated in ethanol and xylenes and mounted using permount.

Pimonidazole staining. Hypoxia staining in the rat prostate tumor was performed using the Hypoxyprobe™-1 plus kit (Hypoxyprobe Inc., Burlington, MA). Hypoxyprobe-1 (pimonidazole HCl) was administered i.p. (120 mg/kg) in tumor bearing rats. Two hours later, the animal was sacrificed; tumor tissue was collected and fixed in 4% formalin solution for 48 h. For detection, tumor sections were incubated with FITC-conjugated mouse monoclonal antibody against pimonidazole (1:50) for overnight at 4˚C. After incubation with primary antibodies, tumor sections were washed thoroughly and visualized using a Zeiss Axio Imager 2 microscope (Carl Zeiss Microscopy, New York, NY) using the FITC filter.

Results

Development of an orthotopic prostate model for multimodal imaging. To appropriately facilitate the study of IGRT for aggressive PCa, it is necessary to have a model that closely mimics human disease, ideally with a tumor that is initially limited to one lobe of the prostate. In this model, we implanted a human prostate tumor cell line which is deficient in a tumor suppressor protein DAB2IP (PC3-KD). This protein is a member of the Ras-GTPase activating family and the loss of DAB2IP has been associated with PI3K-Akt hyperactivation (9), increased radiation resistance (5,6), evasion of apoptosis (9), epithelial-mesenchymal transition and poor clinical outcomes (10). The PC3-KD cells were implanted either using an open surgical method in nude rats (Fig. 1A and B) or a minimally invasive method using ultrasound guidance in Copenhagen rats. Using the open surgical method cells were successfully implanted in all animals (n=17), however when using the ultrasound guided method the successful implantation rate was 70% (n=7). We also placed a gold fiducial marker as shown in Fig. 1C whereas, Fig. 1D shows BL imaging on weeks 1 and 3 after implantation.

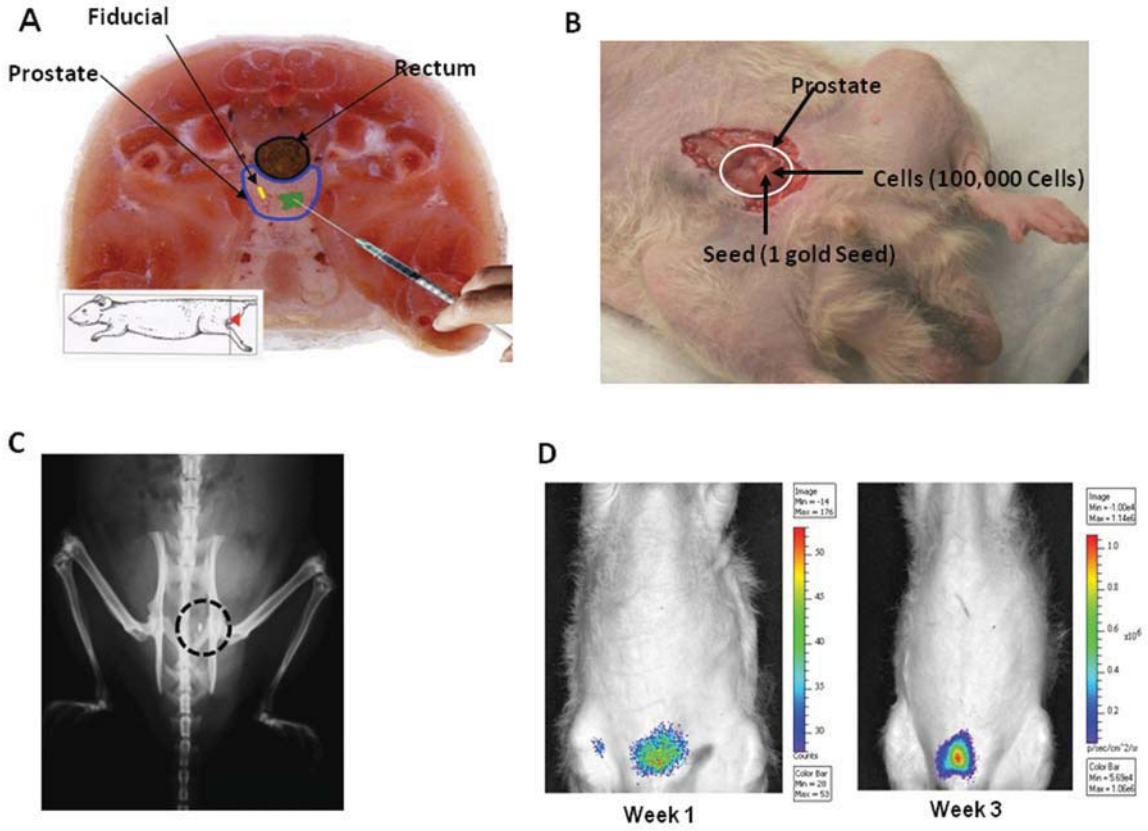

Figure 1. Orthotopic tumor generation in the rat prostate. (A) Transverse section of the rat anatomy showing the location of the prostate and rectum and schematic representation of the implantation of prostate cancer cells and fiducial (Courtesy of: A color atlas of sectional anatomy of rat; Toshiyuki Hayakawa and Takamasa Iwaki). (B) Tumor cells were placed using an open surgical method. The prostate was located by creating an incision into the abdomen and dissecting through the peritoneum. A gold fiducial marker was placed into the right lobe of the prostate using a trocar mounted on an 18 gauge needle and using the same needle, 1 ml syringe was attached and $1x10^5$ PC3-KD cells in 30 μl were injected into the prostate. (C) X-ray of rat pelvis showing the gold fiducial successfully implanted into the prostate. (D) BLI confirming proper implantation of the tumor as well as to track growth.

PC3-KD cells are highly aggressive and demonstrate significant radio-resistance (Fig. 2A). We also performed ultrasound guided PC3-KD cell implantation in Copenhagen rats (Fig. 2B) and then tumor progression was followed by BL imaging (Fig. 2C). Because of the poor inherent contrast between the prostate tissue and tumor, CT is not an optimal imaging modality for determination of size and location of prostate tumors. Therefore, we used ultrasound (Fig. 2D) and MRI to monitor tumor growth, size and location. By using ultrasound, it is possible to create three dimensional reconstructions of the tumor and track the tumor volume. Ultrasound images obtained from this model are notable for areas of necrosis and diffuse calcification throughout the tumor as represented by the varying echogeneity of the image (Fig. 2D).

Fig. 3A displays the high resolution digital image of the OT tumors in the right prostate lobe of a nude rat. A specimen of such tumor was isolated from the prostate with representative sizing and dissection showing grossly visible areas of necrosis (Fig. 3C). We also performed MRI on nude rats (Fig. 3B) and this imaging modality in particular is highly useful for radiation treatment planning (Fig. 3D).

Tumor growth and response to radiation therapy. PC3-KD cells were implanted into the prostate of Copenhagen (immune competent) and athymic nude rats (immune deficient). Tumor growth was followed by BLI as described above. Once the tumor size reached a certain size (approximately 5-7 mm in diameter) based on ultrasound imaging, animals were split into either a treatment (n=2 for Copenhagen; n=6 for Nude Rats, respectively) or control arm (n=2 for both arms). Fig. 4A (upper and lower panel) demonstrates tumor progression in Copenhagen rats after receiving radiation treatment.

Control group tumors demonstrated aggressive, but predictable growth (Fig. 4A, lower panel). We initiated radiation treatment on the rats when the total Flux (photon/sec) (integrated over an appropriate region of interest, ROI) reached approximately $2.6\text{-}3.0x10^5$ as shown in Fig. 4B. We allowed one Copenhagen rat to achieve a slightly larger tumor volume before initiating treatment (Fig. 4B). The rat was treated with 2 fractions of 10 Gy radiation as shown in Fig 4A. Radiation was delivered using image guidance to ensure that dose was delivered to the tumor. Though PC3-KD is an aggressive radioresistant cell line (Fig. 2A), the tumor demonstrated a significant initial response to radiation therapy (Fig. 4A and B). In Copenhagen rats it appears as if the tumors are initially controlled but begin to grow a few weeks after radiation. We noted that BLI signal does not completely resolve, remaining at a detectable level until week 7-8 (Fig. 4B). Between weeks 9-10, a new focus of intensity reappears at the site of the original tumor bed and ultimately grew uncontrollably and the animal died at

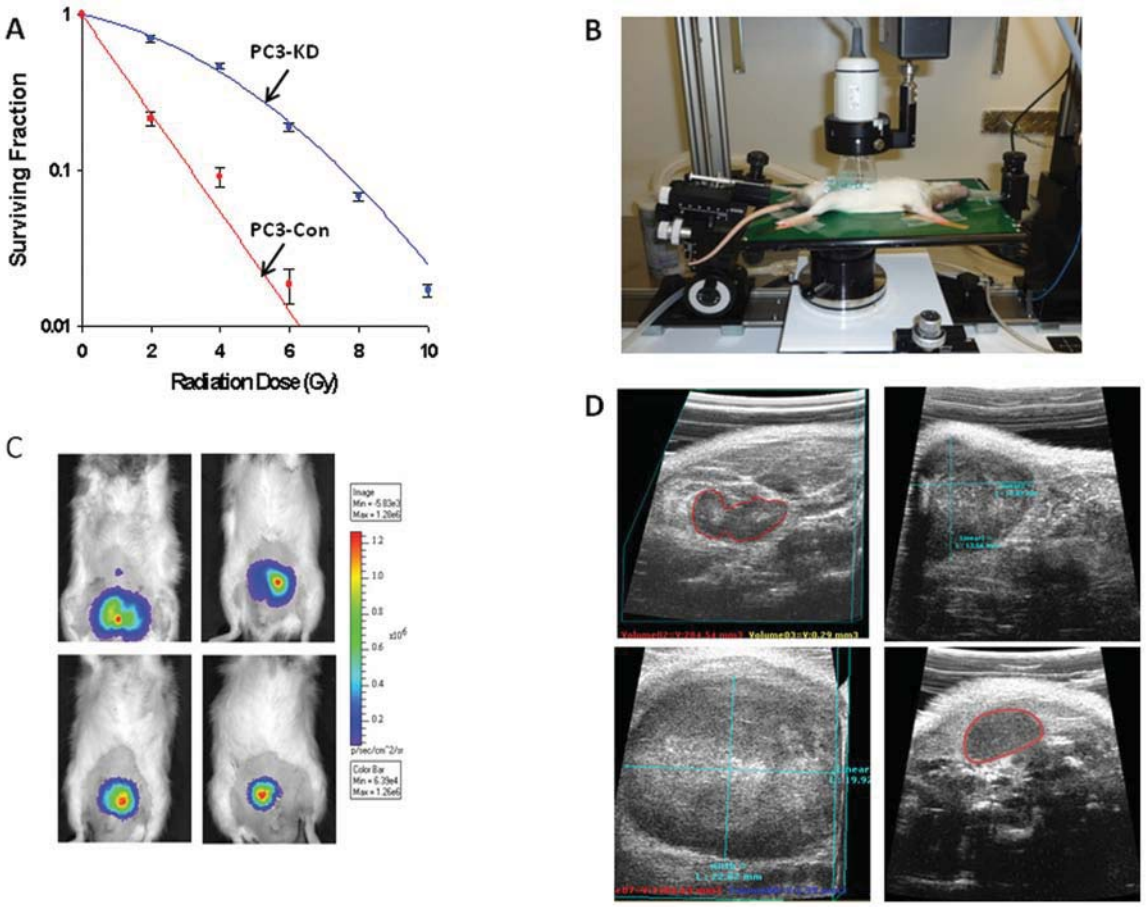

Figure 2. (A) Clonogenic survival assay using a PC3-Con (DAB2IP proficient) PC3-KD (DAB2IP silenced) cell line. (B) Set up of ultrasound imaging station for tumor cell implantation and imaging. (C) BLI of four different Copenhagen rats demonstrating various stages of tumor growth. (D) Ultrasound imaging of prostate as well as proximal pelvic organs. Prostate tumors are outlined in red. Each panel represents an axial ultrasound image of an OT tumor in the prostate. The left upper section of this image is notable for diffuse calcification and necrosis. Tumors reached diameters as large as 2 cm before being euthanized.

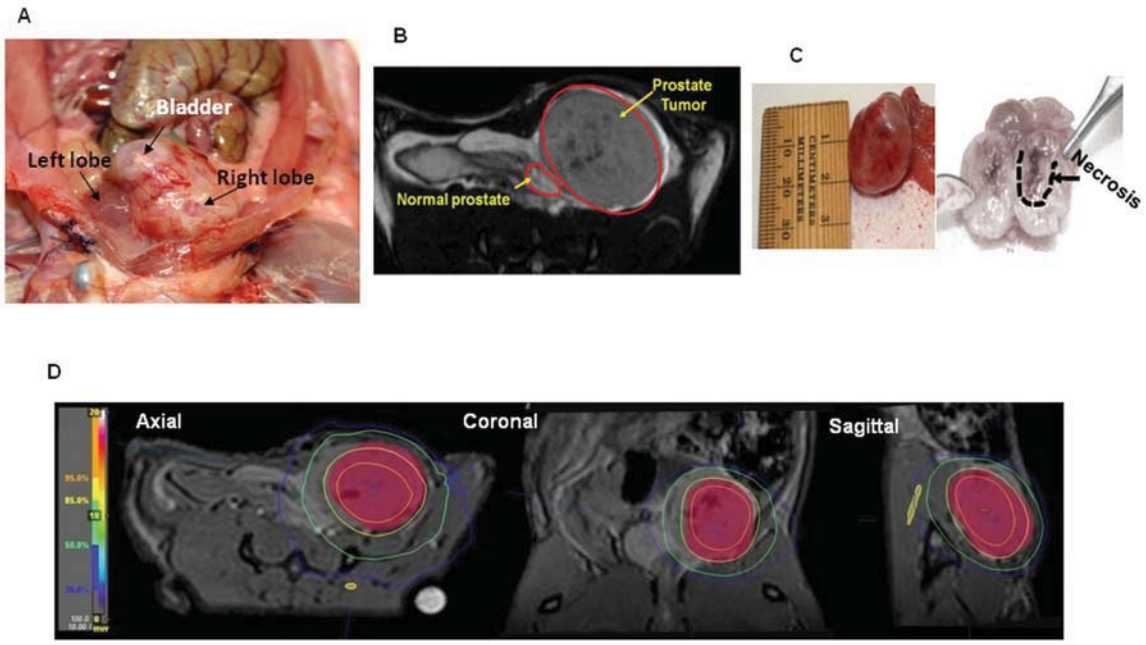

Figure 3. (A) Digital image displaying OT tumors in the rat pelvis after euthanasia. No visible metastasis was observed to other structures within the perineum or peritoneum. (B) MRI provides a non-invasive method to track tumor growth. (C) Specimen tumor resected en bloc with representative sizing. The tumor, once dissected, displays large grossly visible areas of necrosis. (D) MRI was used to create radiation treatment plans for the rats for applying uniform dose.

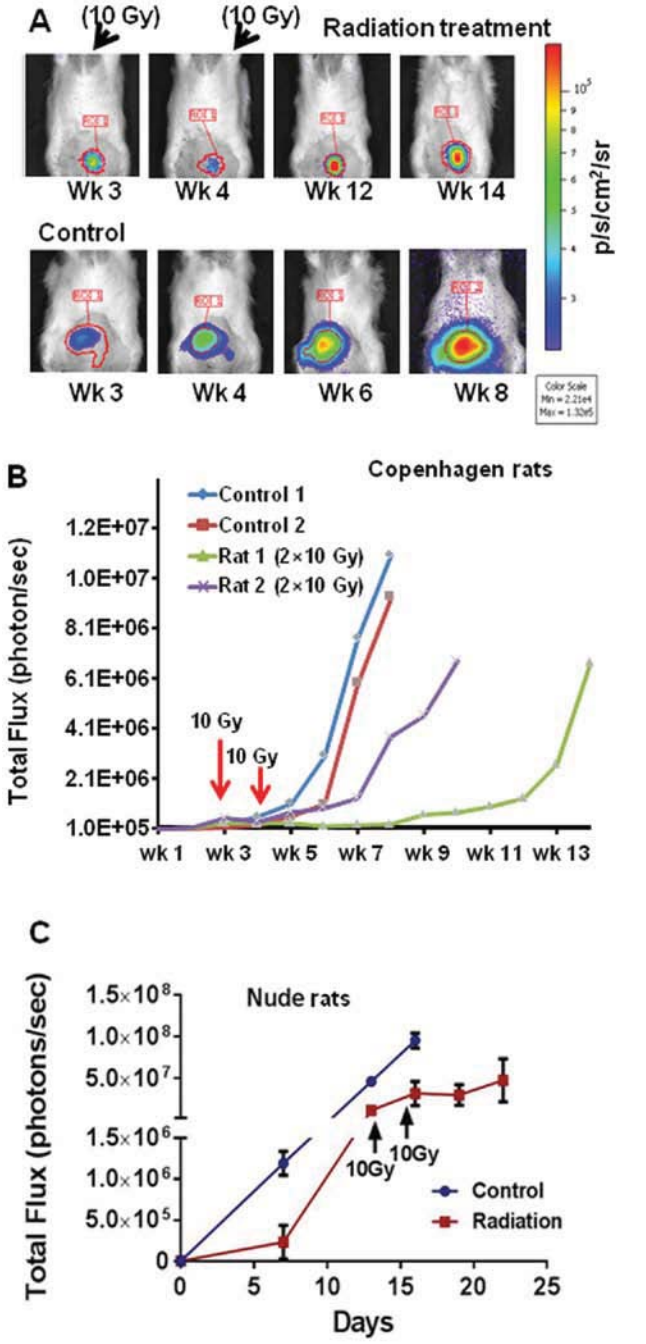

Figure 4. (A) The upper panel displays the tumor growth (rat 1) throughout the treatment course. The lower panel displays with the course of an untreated rat (control 1). The heat scale is given in signal intensity per unit area (p/s/cm^2/sr). (B and C) Tumor growth curve (control and radiation treated) of the (B) Copenhagen rats and (C) Nude rats obtained by integrating the BLI signal (total Flux) over a region of interest. Arrows indicate the days when radiation was delivered.

the end of week 14 (Fig. 4B). The animal with a larger initial tumor (Rat 2) also received a similar dose (total 20 Gy) however, died earlier at week 11. Tumor burden led to compression of the urethra and partial obstruction of the rectum. Therefore, death was caused either by post renal failure or recto-sigmoid perforation secondary to fecalith impaction. However, it is clear that primary tumor caused the complication which led to death. It is also important to note that the peritoneum and mesentery were free of metastatic disease as observed in Fig. 3A. In contrast, rats receiving no radiation BLI signal increased continuously and the animals were euthanized at week 8 (Fig. 4A, lower panel, B).

The athymic nude rat tumors displayed the same aggressive growth pattern, however, they grew significantly faster than the tumors in Copenhagen rats. Control group displayed aggressive, but predictable growth; rats were euthanized on day 16. We initiated radiation as soon as signal appeared in the treatment rats (total Flux photons/sec; $5x10^5$ to $1x10^6$) (Fig. 4C). These rats were also treated with 2x10 Gy on days 13 and 16. Tumors display little response to radiation; ultimately tumor growth was delayed for a matter of days before resuming growth. By day 22 tumors were large enough to warrant euthanasia. Our previous mouse model study also showed that PC3-KD subcutaneous tumors are highly radioresistant when treated with fractionated radiation (6). These results clearly demonstrate that orthotopically implanted PC3-KD cells can recapitulate aggressive prostate tumors and furthermore, if not treated at an early stage, local control is difficult to achieve and this necessitates the use of pathway specific inhibitors in combination with radiation treatment. While possessing intrinsic radiation resistance, we demonstrate that DAB2IP deficient tumors can recur after initial response to appropriate IGRT.

To correlate the imaging with biological events we performed IHC analysis. H&E stained sections confirm the placement of the tumor into the rat prostate; PC3-KD cells are highly anaplastic and aggressive (Fig. 5A). Orthotopically implanted tumors are very similar to human disease, tumors are locally aggressive as shown in Fig. 5C. Radiated rat prostates display gross necrosis and cell death, some areas of the tumor show changes indicative of apoptosis (Fig. 5B and D) these sections agree with the ultrasound findings which were indicative of necrosis. Changes seen in the irradiated rat prostates were consistent with reactive inflammation, neutrophils can be seen infiltrating the perivascular space as well as infiltrating the areas of necrosis (Fig. 5E). Using pimonidazole, we show that tumors develop large areas of hypoxia heterogeneously spread throughout the tumor (Fig. 5F). These areas of hypoxia may explain the high amount of resistance to radiation therapy.

Discussion

While several other OT prostate tumors have been reported in the literature (11-13), there are currently no models that can accurately represent tumors that fail initial RT. With the increased use of genetic manipulation leading towards the addition of luciferase reporters to cell lines, it is now feasible to track tumor growth and response to treatment. Given that there is a lack of effective therapies for patients who present with biochemical failure, we felt that developing an aggressive locally advanced model that did not respond to radiation therapy alone was necessary to develop combined modality therapies capable of controlling aggressive tumors.

There are several requirements necessary for the development of a locally advanced prostate tumor specially for IGRT or combined modality therapy. Current OT prostate models for preclinical studies are primarily developed in mouse, however, to delineate tumors and track tumor response animals with larger prostates need to be used, hence we used rats. Secondly, the major difficulty in creating an OT model that accurately demonstrates

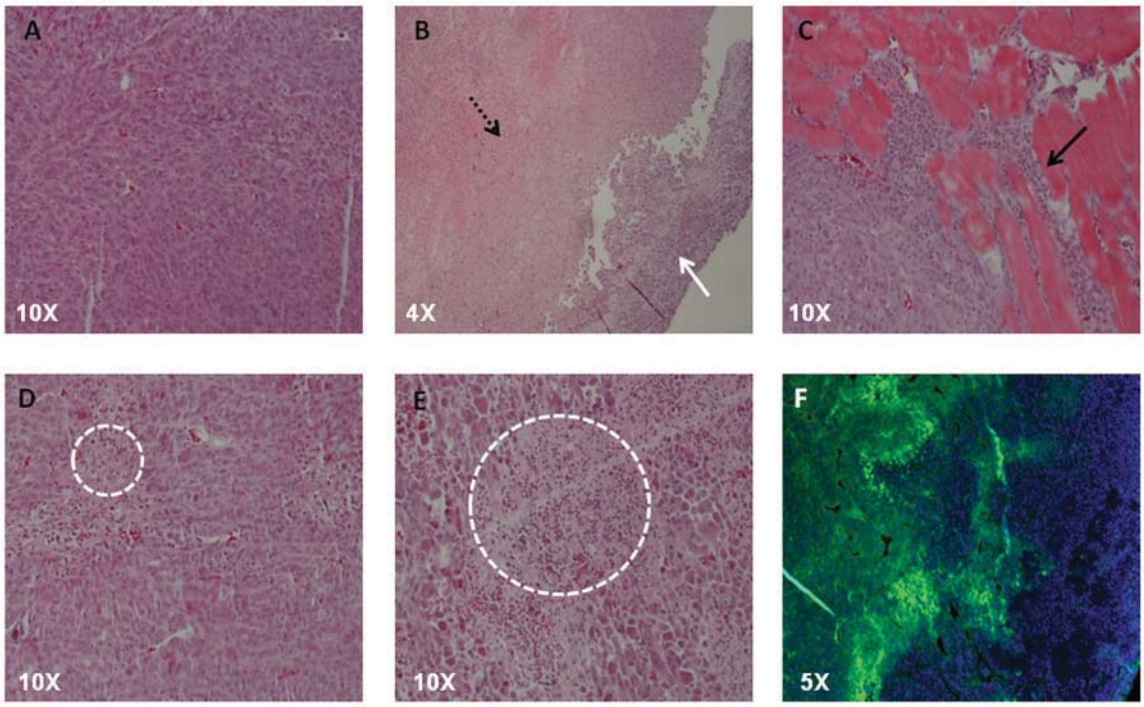

Figure 5. (A) H&E stained tissue section from a non-irradiated control; PC3-KD tumors are highly anaplastic and aggressive with high nuclear to cytoplasmic ratios, loss of cell polarity and loss of glandular structure. (B) H&E stained tissue section from an irradiated tumor. The irradiated area is highly necrotic (black dash arrow) displaying loss of cellular structure and high levels of eosin staining as compared to a strip of unirradiated tissue (white arrow). (C) H&E section of tumor showing invasion into adjacent skeletal muscle, the black arrow delineates tumor cells invading longitudinally down a skeletal muscle fascicle. (D) H&E section notable for areas of apoptosis. Apoptotic cells are noted for the loss of cellular detail as well as pyknotic nuclei (white dashed circle). (E) H&E image of radiated sections of tumor showing infiltration by neutrophils and macrophages in the early periods are radiation (white dashed circle), these areas will eventually become fibrotic. (F) Immunofluorescence using FITC conjugated antibodies against pimonidazole. Areas that are stained green represent areas of hypoxia, blue areas represent cell nuclei (DAPI). PC3-KD tumors show strong areas of central core hypoxia.

human disease, specifically a tumor that is radiation resistant, is reliability. In order to facilitate resistance we used a DAB2IP knockdown prostate cell line. By using the DAB2IP knockdown cell line resistant tumors are reliably formed. Orthotopically implanted cells were able to grow large tumors in immune-competent male Copenhagen rats as well as nude rats.

Copenhagen rats are used primarily to study metastatic progression of prostate cancer as first described by Dunning (14-16). Several of the models developed to study prostate carcinoma did involve the injection of cells into the prostate (16), however, previous studies were done using syngeneic models which did not invoke a strong response when orthotopically implanted (17,18). Previous studies also investigated the radiation sensitivity of the Copenhagen rat prostate tumor model, which consists of anaplastic high grade tumors (15), and found that the tumors had radioresistant subpopulations *in vitro* but could not find correlating aggressive radiation resistant tumors *in vivo* (19). Furthermore, previous studies could not recapitulate recurrent disease (19).

It is very interesting to note the differences in growth rates between immune competent Copenhagen rats and athymic nude rats. Tumors in nude rats grow much quicker causing mass effect within days rather than weeks. Paradoxically, the rapidly growing nude rat tumors should be more radiation sensitive, however, our model shows that they are much more radiation resistant. It is possible that innate immunity, rather than humoral immunity, response of Copenhagen rats plays a significant role in controlling tumor proliferation. However, the Copenhagen study remains a pilot and this requires a larger more in depth study.

Once the tumors were successfully implanted they exhibited several characteristics pertinent to aggressive tumor growth. Radiation response also seems to correlate to initiation of treatment. In Copenhagen rats, treatment arm that received RT early regrowth is delayed by several weeks. However, the animal with the larger starting volume relapse was significantly shorter indicating that if treatment is delayed the tumor becomes more difficult to control. It is also important to note that based on the calculated α- and β-values of PC3-KD 2 fractions of 10 Gy leads to an LQED (Linear Quadratic Equivalent Dose) 2 Gy of 60 Gy, a dose that is clinically relevant in the treatment of human PCa. Furthermore, rapidly growing tumors often display heterogeneous areas of necrosis as a result of insufficient vascular supply (20). Insufficient blood supply leads to hypoxia which correlates to poor response. Ultrasound imaging of large tumors demonstrate large areas of necrosis as well as diffuse calcification and pimonidazole staining confirms that implanted tumors rapidly develop several large hypoxic areas.

In radiation resistant models, the ability to track tumor growth and response to therapy is essential. BLI was the primary imaging modality in this study and has been correlated with both CT as well as MRI (21). We further evaluated our model through the use of ultrasound. Here we demonstrate that ultrasound technology can be used successfully for the determination of tumor volume as well as to aid in tumor cell implantation.

Ultrasound was also helpful in revealing additional information regarding the accurate localization, calcification, necrosis and the effects of the tumor on proximal pelvic organs such as bladder, which are not appreciable on BLI. While both imaging modalities could be used individually, the complementary information provided using both modalities creates a complete image of the tumor.

Acknowledgements

We thank Ralph Mason, at UT Southwestern Medical Center for providing the Copenhagen Rats; Ramona Lopez and Thomas Boike for imaging assistance; Scott Buttars at Visual Sonics for technical assistance in ultrasound. This study was supported by the funding from Flight Attendant Medical Research Institute (D.S.), W81XWH-11-1-0270 (D.S.). Additional support for this study in part through the UT Southwestern Small Animal Imaging Research Program (UTSWSAIRP; U24 CA12660801, P20 Pre-ICMIC CA86354) and UT Southwestern Clinical and Translational Science Award grant 5TL1 RR024984 (V.T.).

References

1. Jemal A, Siegel R, Xu J and Ward E: Cancer statistics, 2010. CA Cancer J Clin 60: 277-300, 2010.
2. Coen JJ, Zietman AL, Thakral H and Shipley WU: Radical radiation for localized prostate cancer: local persistence of disease results in a late wave of metastases. J Clin Oncol 20: 3199-3205, 2002.
3. Li T, Thongphiew D, Zhu X, *et al*: Adaptive prostate IGRT combining online re-optimization and re-positioning: a feasibility study. Phys Med Biol 56: 1243-1258, 2011.
4. De Crevoisier R, Tucker SL, Dong L, *et al*: Increased risk of biochemical and local failure in patients with distended rectum on the planning CT for prostate cancer radiotherapy. Int J Radiat Oncol Biol Phys 62: 965-973, 2005.
5. Kong Z, Xie D, Boike T, *et al*: Downregulation of human DAB2IP gene expression in prostate cancer cells results in resistance to ionizing radiation. Cancer Res 70: 2829-2839, 2010.
6. Kong Z, Raghavan P, Xie D, *et al*: Epothilone B confers radiation dose enhancement in DAB2IP gene knock-down radioresistant prostate cancer cells. Int J Radiat Oncol Biol Phys 78: 1210-1218, 2010.
7. Pidikiti R, Stojadinovic S, Speiser M, *et al*: Dosimetric characterization of an image-guided stereotactic small animal irradiator. Phys Med Biol 56: 2585-2599, 2011.
8. Saha D, Watkins L, Yin Y, *et al*: An orthotopic lung tumor model for image-guided microirradiation in rats. Radiat Res 174: 62-71, 2010.
9. Xie D, Gore C, Zhou J, *et al*: DAB2IP coordinates both PI3K-Akt and ASK1 pathways for cell survival and apoptosis. Proc Natl Acad Sci USA 106: 19878-19883, 2009.
10. Xie D, Gore C, Liu J, *et al*: Role of DAB2IP in modulating epithelial-to-mesenchymal transition and prostate cancer metastasis. Proc Natl Acad Sci USA 107: 2485-2490, 2010.
11. Raheem O, Kulidjian AA, Wu C, *et al*: A novel patient-derived intra-femoral xenograft model of bone metastatic prostate cancer that recapitulates mixed osteolytic and osteoblastic lesions. J Transl Med 9: 185, 2011.
12. Shikanov S, Shikanov A, Gofrit O, Nyska A, Corn B and Domb AJ: Intratumoral delivery of paclitaxel for treatment of orthotopic prostate cancer. J Pharm Sci 98: 1005-1014, 2009.
13. Tse BW, Russell PJ, Lochner M, Forster I and Power CA: IL-18 inhibits growth of murine orthotopic prostate carcinomas via both adaptive and innate immune mechanisms. PLoS One 6: e24241, 2011.
14. Dunning WF: Prostate cancer in the rat. Natl Cancer Inst Monogr 12: 351-369, 1963.
15. Lubaroff DM and Culp DA: Experience with an animal model for the study of prostatic carcinoma. Trans Am Assoc Genitourin Surg 69: 72-77, 1977.
16. Lubaroff DM, Canfield L, Feldbush TL and Bonney WW: R3327 adenocarcinoma of the Copenhagen rat as a model for the study of the immunologic aspects of prostate cancer. J Natl Cancer Inst 58: 1677-1689, 1977.
17. Lopez DM and Voigt W: Adenocarcinoma R-3327 of the Copenhagen rat as a suitable model for immunological studies of prostate cancer. Cancer Res 37: 2057-2061, 1977.
18. Vieweg J, Rosenthal FM, Bannerji R, *et al*: Immunotherapy of prostate cancer in the Dunning rat model: use of cytokine gene modified tumor vaccines. Cancer Res 54: 1760-1765, 1994.
19. Rao BR, Slotman BJ, Geldof AA and Perez CA: Radiation sensitivity of Copenhagen rat prostatic carcinoma (R3327-AT and R3327-MATLyLu). Int J Radiat Oncol Biol Phys 20: 981-985, 1991.
20. Vaupel P, Kallinowski F and Okunieff P: Blood flow, oxygen and nutrient supply, and metabolic microenvironment of human tumors: a review. Cancer Res 49: 6449-6465, 1989.
21. Szentirmai O, Baker CH, Lin N, *et al*: Noninvasive bioluminescence imaging of luciferase expressing intracranial U87 xenografts: correlation with magnetic resonance imaging determined tumor volume and longitudinal use in assessing tumor growth and antiangiogenic treatment effect. Neurosurgery 58: 365-372, 2006.